Biochemistry **42,** 1890–1899
39. Getzoff, E. D., Tainer, J. A., Stempien, M. M., Bell, G. I., and Hallewell, R. A. (1989) *Proteins* **5,** 322–336
40. Cardoso, R. M., Thayer, M. M., DiDonato, M., Lo, T. P., Bruns, C. K., Getzoff, E. D., and Tainer, J. A. (2002) *J. Mol. Biol.* **324,** 247–256
41. Tiwari, A., and Hayward, L. J. (2003) *J. Biol. Chem.* **278,** 5984–5992
42. Aoki, M., Ogasawara, M., Matsubara, Y., Narisawa, K., Nakamura, S., Itoyama, Y., and Abe, K. (1993) *Nat. Genet.* **5,** 323–324
43. Cudkowicz, M., McKenna-Yasek, D., Sapp, P., Chin, W., Geller, B., Hayden, D., Horvtiz, H., and Brown, R. (1997) *Ann. Neurol.* **41,** 210–212
44. Nagai, M., Aoki, M., Miyoshi, I., Kato, M., Pasinelli, P., Kasai, N., Brown, R. H., Jr., and Itoyama, Y. (2001) *J. Neurosci.* **21,** 9246–9254
45. Miyazaki, K., Fujita, T., Ozaki, T., Kato, C., Kurose, Y., Sakamoto, M., Kato, S., Goto, T., Itoyama, Y., Aoki, M., and Nakagawara, A. (2004) *J. Biol. Chem.* **279,** 11327–11335
46. Rodriguez, J. A., Valentine, J. S., Eggers, D. K., Roe, J. A., Tiwari, A., Brown, R. H., Jr., and Hayward, L. J. (2002) *J. Biol. Chem.* **277,** 15932–15937
47. Prusiner, S. B. (1998) *Proc. Natl. Acad. Sci. U. S. A.* **95,** 13363–13383

Am J Physiol Cell Physiol 288: C253–C259, 2005.
First published September 29, 2004; doi:10.1152/ajpcell.00014.2004.

Overexpression of mutated Cu,Zn-SOD in neuroblastoma cells results in cytoskeletal change

Rina Takamiya,[1] Motoko Takahashi,[1] Yong Seek Park,[1] Yoshie Tawara,[1] Noriko Fujiwara,[2] Yasuhide Miyamoto,[1] Jianguo Gu,[1] Keiichiro Suzuki,[2] and Naoyuki Taniguchi[1]

[1]*Department of Biochemistry, Osaka University Graduate School of Medicine, Osaka, Japan; and* [2]*Department of Biochemistry, Hyogo College of Medicine, Hyogo, Japan*

Submitted 9 January 2004; accepted in final form 21 September 2004

Takamiya, Rina, Motoko Takahashi, Yong Seek Park, Yoshie Tawara, Noriko Fujiwara, Yasuhide Miyamoto, Jianguo Gu, Keiichiro Suzuki, and Naoyuki Taniguchi. Overexpression of mutated Cu,Zn-SOD in neuroblastoma cells results in cytoskeletal change. *Am J Physiol Cell Physiol* 288: C253–C259, 2005. First published September 29, 2004; doi:10.1152/ajpcell.00014.2004.—Amyotrophic lateral sclerosis (ALS) involves the progressive degeneration of motor neurons in the spinal cord and the motor cortex. It has been shown that 15–20% of patients with familial ALS (FALS) have defects in the *Sod1* gene, which encodes Cu,Zn-superoxide dismutase (SOD). To elucidate the pathological role of mutated Cu,Zn-SOD, we examined the issue of whether mutated Cu,Zn-SOD affects the cell cycle. Mouse neuroblastoma Neuro-2a cells were transfected with human wild-type or mutated (G37R, G93A) Cu,Zn-SOD. Mutated, Cu,Zn-SOD-transfected cells exhibited marked retardation in cell growth and G_2/M arrest. They also displayed lower reactivity to phalloidin, indicating that the cytoskeleton was disrupted. Immunoprecipitation, two-dimensional gel electrophoresis, and Western blot analysis indicated that mutated Cu,Zn-SOD associates with actin. Similar results were obtained by in vitro incubation experiments with purified actin and mutated Cu,Zn-SOD (G93A). These results suggest that mutated Cu,Zn-SOD in FALS causes cytoskeletal changes by associating with actin, which subsequently causes G_2/M arrest and growth retardation.

amyotrophic lateral sclerosis; copper; zinc superoxide dismutase; G_2/M arrest; neurodegenerative disease

AMYOTROPHIC LATERAL SCLEROSIS (ALS) is a neurodegenerative disease characterized by the selective and progressive dysfunction of motor neurons initiated in middle-aged adults (1). The pathology of the disease results from the death of lower motor neurons in the brainstem and spinal cord and upper motor neurons in the cerebral cortex. Approximately 5–10% of ALS cases are familial ALS (FALS), and among FALS cases, 15–20% have been linked to autosomal dominant inheritance of mutations in Cu,Zn-superoxide dismutase (Cu,Zn-SOD) (10, 30). Cu,Zn-SOD functions as an antioxidative enzyme that catalyzes the conversion of $O_2^-\cdot$ to hydrogen peroxide, which is further detoxified by other antioxidant enzymes such as catalase and glutathione peroxidase. More than 100 types of mutations in Cu,Zn-SOD, which comprises 153 amino acids, have been reported to be associated with the FALS (10). Although some FALS-related mutants show reduced enzymatic activities, many retain full activity (26). Furthermore, transgenic mice that have FALS-associated *Sod1* mutations develop FALS-like symptoms despite elevated Cu,Zn-SOD activity, suggesting that the disease is not caused by the loss of normal enzymatic activity (15). Thus the motor neuron dysfunction observed in FALS is generally thought to be due to the newly acquired neurotoxicity of mutant Cu,Zn-SOD. Several hypotheses have been proposed to explain this toxic gain of function of mutated Cu,Zn-SOD in FALS (6, 18, 19, 29). For example, oxidative stress produced by aberrant catalysis (13, 36), abnormal Cu chemistry (26), decreased glutamate metabolism (6), and increased cytoplasmic aggregation (7, 11, 18, 20, 26, 29) have been studied in the setting of mutated Cu,Zn-SOD. However, the precise mechanism of pathogenesis is not understood.

A pathological hallmark of both sporadic and familial ALS involves the abnormal accumulation of cytoskeletal proteins such as neurofilament, tubulin, and actin in the perikaryon and axon of motor neurons (12, 17, 19, 31). Recent studies have reported that these cytoskeletal changes induce slowing of axonal transport in mutated Cu,Zn-SOD transgenic mice (37).

Previous reports demonstrated that the abnormal regulation of mitotic proteins and an aberrant cell cycle have been observed in neurodegenerative diseases, including Alzheimer's disease and ALS. In those studies, it was suggested that cell cycle signaling may affect the neuronal death pathway (25, 33). Thus we hypothesized that the cell cycle might be affected by mutated Cu,Zn-SOD in FALS.

In this study, mouse neuroblastoma cells were transfected with mutated Cu,Zn-SOD. The mutated Cu,Zn-SOD transfectants grew at a much slower rate than the wild-type transfectants or mock transfectants, and G_2/M arrest was observed in the mutant transfectants. As evidenced by confocal microscopy, cytoskeletal destruction occurred in the mutant transfectants. The issue of how mutated Cu,Zn-SOD affected cytoskeletal components was examined.

MATERIALS AND METHODS

Cell culture and transfection. Neuro-2a (N2a) cells, a mouse neuroblastoma cell line, were grown in DMEM (Sigma, St. Louis, MO) supplemented with 10% fetal bovine serum. Mutated Cu,Zn-SOD cDNA, designated G37R and G93A, were constructed using site-directed mutagenesis with a uracil template as described previously (14). The DNA fragments were ligated to a mammalian expression vector, pcDNA3.1/Zeo (Invitrogen, Carlsbad, CA), which was regulated by the cytomegalovirus promoter. The resulting plasmids were transfected into N2a cells using Lipofectamine reagent (Life Technologies/Invitrogen) according to the manufacturer's instruc-

Address for reprint requests and other correspondence: N. Taniguchi, Dept. of Biochemistry, Osaka Univ. Graduate School of Medicine, B1, 2-2 Yamadaoka, Suita, Osaka 565-0871, Japan (E-mail: proftani@biochem.med.osaka-u.ac.jp).

The costs of publication of this article were defrayed in part by the payment of page charges. The article must therefore be hereby marked "*advertisement*" in accordance with 18 U.S.C. Section 1734 solely to indicate this fact.

0363-6143/05 $8.00 Copyright © 2005 the American Physiological Society

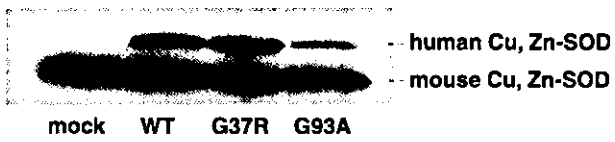

Fig. 1. Characterization of human wild-type and mutated Cu,Zn-superoxide dismutase (SOD) in transfectants of Neuro-2a (N2a) cells, a mouse neuroblastoma cell line. Cell lysates (10 μg) were subjected to 15% SDS-PAGE and subsequent Western blot analysis using an anti-human Cu,Zn-SOD antibody. Mock, mock transfectant; WT, wild-type Cu,Zn-SOD transfectant; G37R, G37R-mutated Cu,Zn-SOD transfectant; G93A, G93A-mutated Cu,Zn-SOD transfectant.

tions. Selection was performed in a medium that contained 1.0 mg/ml Zeocin (GIBCO-BRL/Invitrogen), and, after a 2-wk incubation, several stable colonies were isolated.

Western blot analysis. N2a cells were lysed in buffer [20 mM Tris·HCl, pH 7.4, 150 mM NaCl, 5 mM EDTA, 1% (wt/vol) Nonidet P-40, 1% (wt/vol) Triton, 10% (wt/vol) glycerol, 5 mM sodium pyrophosphate, 10 mM NaF, 1 mM sodium orthovanadate, 10 mM β-glycerophosphate, and 1 mM dithiothreitol (DTT)] with protease inhibitors. Protein (10 μg) was subjected to 15% SDS-PAGE. For Western blot analysis using an anti-Cu,Zn-SOD antibody, the proteins were transferred to nitrocellulose membranes (Schleicher & Schuell, Keene, NH). The blots were blocked with 5% skim milk and 2% BSA and then probed with goat anti-human Cu,Zn-SOD (2). After incubation with a peroxidase-conjugated secondary antibody, immunoreactive bands were visualized using an enhanced chemiluminescence kit (Amersham Biosciences, Piscataway, NJ).

Cell growth curve. Equal numbers (5×10^4) of mock, wild-type, G37R, and G93A Cu,Zn-SOD transfected cells were plated onto six-well tissue culture dishes, and the cell number was determined by hemocytometric counting at 0, 1, 2, and 3 days after cell plating. Triplicate plates were used for each time point (22).

Determination of cell cycle by image analysis. The relative number of cells occupying a particular state of the cell cycle at a specific time was obtained by staining cells with the DNA intercalator propidium iodide (5 μg/ml). Stoichiometric binding resulted when the cells were fixed in cold 70% ethanol for at least 6 h, followed by two washes with PBS and incubation with 100 μg/ml RNase for 30 min at 37°C and two additional washes with PBS (22). Single-parameter histograms were generated by analyzing the cells on a FACStarPlus flow cytometer (BD Biosciences Immunocytometry Systems, San Jose, CA).

Confocal laser scanning microscopy. Cells grown on glass-bottom dishes were fixed with 2% paraformaldehyde-PBS for 10 min on ice. Cells were rinsed in PBS and then treated with 1% saponin for membrane permeabilization. The cells were incubated with 100 ng/ml of tetramethyl rhodamine isothiocyanate (TRITC)-labeled phalloidin (Sigma) or FITC-labeled anti-tubulin antibody (Sigma) for 2 h at room temperature. After washing with PBS with 0.05% Triton five times, the cells were analyzed using confocal laser microscopy. To identify the nuclei, cells were stained with propidium iodide, the size of the nuclei was measured through the microscope, and the image was processed digitally using an eight-bit image analyzer (NIH Image software, version 1.63).

Immunoprecipitation, two-dimensional gel electrophoresis and Western blotting. For the immunoprecipitation of Cu,Zn-SOD or actin, whole cell lysates were incubated with 4 μg of goat anti-human Cu,Zn-SOD antibody or mouse anti-actin antibody (Sigma) and 15 μl of protein G-Sepharose 4 Fast Flow (Amersham Biosciences) for 12 h at 4°C (32). For two-dimensional (2-D) gel electrophoretic analysis, immunoprecipitates were incubated with immobilized pH gradient (IPG) buffer {8 M urea, 2% (wt/vol) 3-([3-cholamidopropyl]dimethylammonio)-2-hydroxy-1-propanesulfonate, 0.5% (vol/vol) carrier ampholyte, pH 3–10, 10 mM DTT, and a trace amount of bromophenol blue} for 4 h. After the samples were centrifuged, the supernatants were subjected to isoelectric focusing using the IPGphor system (Amersham Biosciences) and a 7-cm IPG strip (pH range, 3–10). The IPG strip was then applied to an SDS-PAGE gel (10 or 15%). The gels were subjected to silver staining using the Silver Stain II kit (Daiichi Pure Chemicals, Tokyo, Japan). Western blotting was performed as described above using an anti-Cu,Zn-SOD antibody or an anti-actin antibody.

Purification of Cu,Zn-SOD produced from Sf21 cells. Recombinant Cu,Zn-SOD was isolated from *Spodoptera frugiperda* 21 (Sf21) cells as described previously (34). Briefly, wild-type and mutated Cu,Zn-SOD expression vectors were transfected into Sf21 cells to produce a recombinant virus. For the production of active Cu,Zn-SOD, aqueous solutions of $CuCl_2$ and $ZnCl_2$ were added directly to the medium until reaching a concentration of 1 mM after viral infection. Infected cells ($n = 4 \times 10^8$) were lysed at 4°C in a hypotonic buffer containing 2.5 mM potassium phosphate, pH 7.4, 1 mM benzamidine, and 0.1 mM *p*-amidinophenylmethanesulfonyl fluoride (Wako Pure Chemical Industries, Osaka, Japan). After homogenization and centrifugation at 100,000 *g* for 1 h, the supernatant was subjected to a DE52 ion exchange column chromatography (Whatman, Brentford, UK) in 2.5 mM K^+-phosphate, pH 7.4. Bound proteins were eluted with a linear gradient of K^+-phosphate from 2.5 to 200 mM. To further purify the enzyme, column chromatography was performed on a hydroxyapatite type I column (Bio-Rad, Hercules, CA) with a liner gradient of K^+-phosphate from 10 to 500 mM using Akta Explorer 10s (Amersham Biosciences).

Assay of actin polymerization. An actin polymerization assay was performed in the presence and absence of Cu,Zn-SOD using an Actin Polymerization Biochem kit (Cytoskeleton, Denver, CO) according to the manufacturer's instructions. The samples also were examined by performing immunoprecipitation with anti Cu,Zn-SOD antibody followed by Western blotting using anti-actin antibody.

Statistical evaluation. Differences among mean values were determined by performing one-way ANOVA with Fisher's multiple-comparison test. $P < 0.05$ was considered statistically significant.

RESULTS

Establishment of N2a clones stably expressing wild-type or mutant human Cu,Zn-SOD. N2a cells were stably transfected with wild-type or mutant Cu,Zn-SOD (G37R, G93A), and five

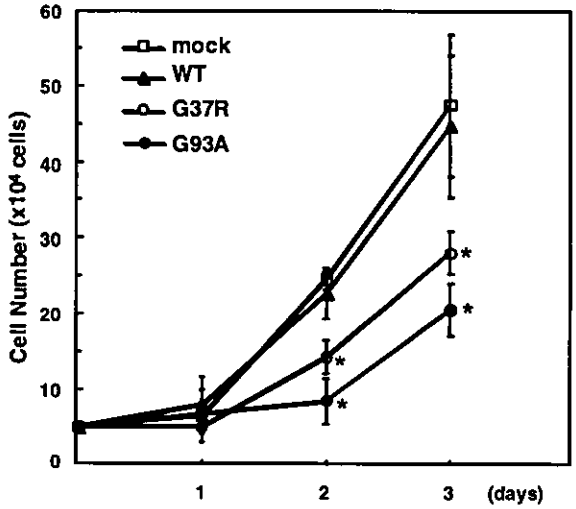

Fig. 2. Growth curves for wild-type or mutated Cu,Zn-SOD-transfected N2a cells. Equal numbers ($n = 5 \times 10^4$ cells) of mock, wild-type, G37R, and G93A Cu,Zn-SOD-transfected cells were plated onto 6-well tissue culture dishes and incubated in DMEM containing 10% FBS. Cell numbers were determined by hemocytometric counting at 0, 1, 2, and 3 days. Each data point is the average of 4 independent experiments. *$P < 0.05$ vs. wild-type Cu,Zn-SOD transfectant.

Zeocin-resistant clones were selected for each cell type. As shown in Fig. 1, the expression levels of Cu,Zn-SOD were verified by Western blot analysis. The upper bands are human enzymes, and the lower bands are endogenous mouse enzymes, as judged by the molecular mass. Because we could not obtain high-expression clones for G93A, the data with indicated clones in Fig. 1 are shown in subsequent figures.

Cell growth arrest in mutant Cu,Zn-SOD-transfected N2a cells. When cell growth was examined, marked inhibition in cell growth was observed in G37R and G93A Cu,Zn-SOD-transfected cells compared with wild-type Cu,Zn-SOD- and mock-transfected cells (Fig. 2). Wild-type Cu,Zn-SOD transfectants showed a growth curve that was similar to that of the mock transfectants. We further determined the cell cycle by conducting flow cytometric analysis. After subconfluent cells were incubated in medium with or without 10% FBS for 48 h, the cells were stained with propidium iodide and subjected to flow cytometric analysis. As shown in Fig. 3*A*, no significant differences were found among mock, wild-type, and mutant Cu,Zn-SOD transfectants in the G_0/G_1 and S phases when grown in a medium containing 10% serum. However, a higher percentage of G37R or G93A Cu,Zn-SOD transfectants was found in the G_2/M phase than with the mock or wild-type Cu,Zn-SOD transfectants. When the cells were subjected to serum starvation, the difference became more obvious; a higher percentage of mock and wild-type Cu,Zn-SOD transfectants was found in the G_0 phase compared with the G37R or G93A Cu,Zn-SOD transfectants, whereas a higher percentage of the mutant transfectants was found in the G_2/M phase compared with mock or wild-type transfectants (Fig. 3*B*). These results suggest that G_2/M arrest occurred with the G37R or G93A Cu,Zn-SOD transfectants.

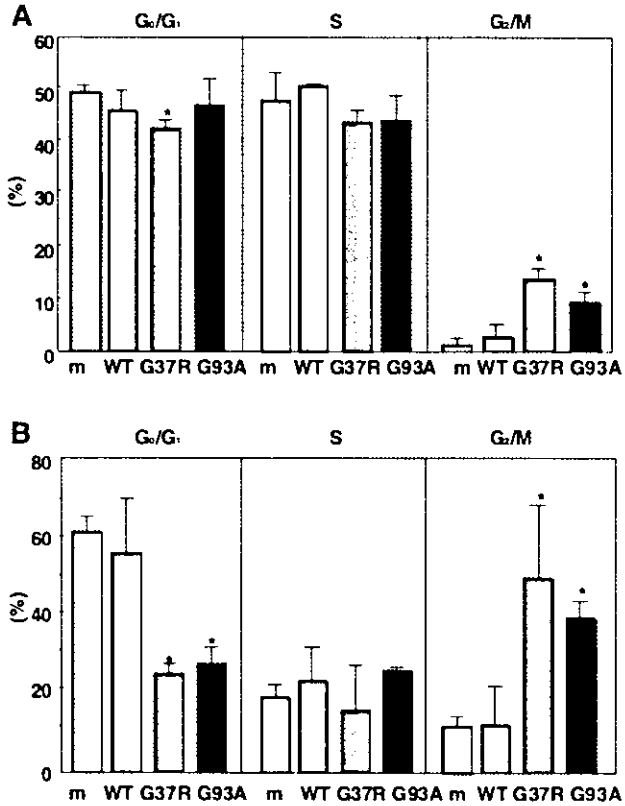

Fig. 3. Cell cycle analysis of wild-type and mutated Cu,Zn-SOD-transfected N2a cells. Cells were incubated in DMEM containing 10% FBS for 1 day and then incubated with or without serum for an additional 48 h. Cell cycles were determined by staining with propidium iodide and by performing flow cytometric analysis. *A*: cells incubated with DMEM containing 10% FBS. *B*: cells were serum starved for 48 h. m, mock transfectant. $^*P < 0.05$ vs. mock transfectant.

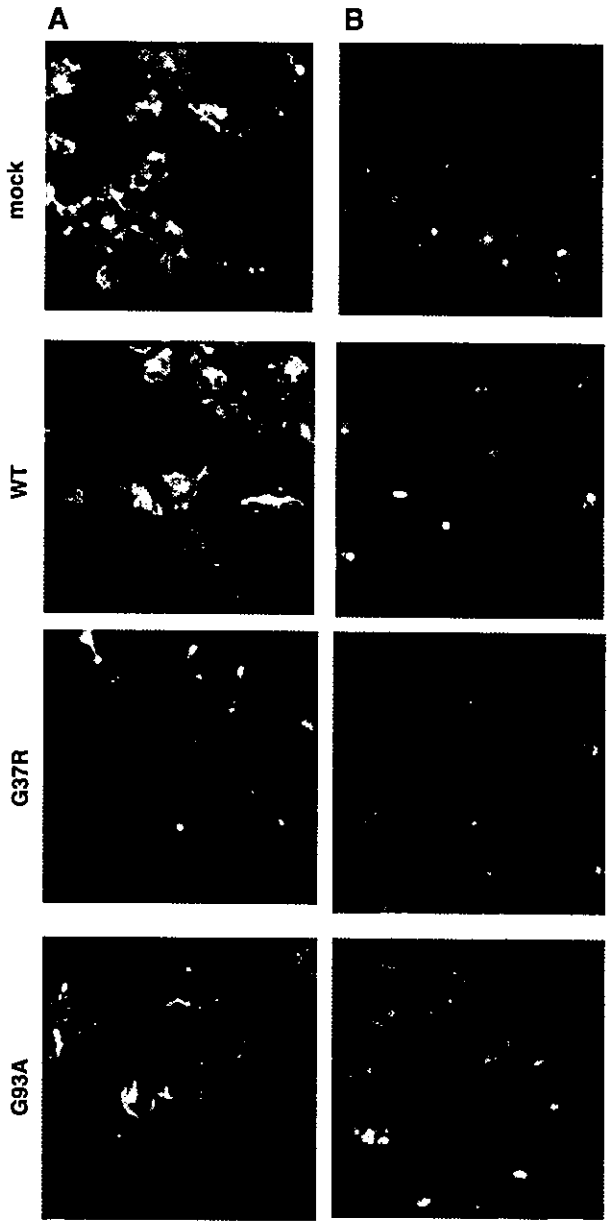

Fig. 4. Determination of cytoskeletal changes in wild-type and mutated Cu,Zn-SOD-transfected N2a cells. After cells were serum starved for 2 days, they were fixed with 2% paraformaldehyde. Florescent images are shown with tetramethylrhodamine isothiocyanate (TRITC)-labeled phalloidin and FITC-labeled anti-α-tubulin antibody. *A*: cells stained with TRITC-labeled phalloidin. *B*: cells stained with FITC-labeled α-tubulin antibody (green) and propidium iodide (red) to identify nuclei. mock, mock transfectant.

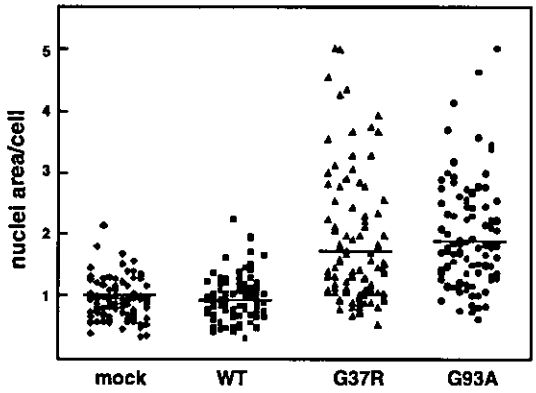

Fig. 5. The size of nuclei in wild-type and mutated Cu,Zn-SOD-transfected N2a cells. After serum starvation for 2 days, the cells were stained with propidium iodide to identify the nucleus. After 100 cells from each culture were randomly collected, the size of the nucleus per cell was measured through the microscope and the image was processed digitally with an 8-bit image analyzer (NIH Image version 1.62). The line in each column indicates the mean value. mock, mock transfectant.

Loss of actin polymerization in mutated, Cu,Zn-SOD-transfected cells. One of the characteristics of the cytoskeletal structure in the M phase is the formation of a contractile ring by actin filaments. The G_2/M arrest observed in mutant transfectants prompted us to examine whether these cells could contain structurally modified actin. After 2-day serum starvation, polymerized actin fiber was stained with phalloidin and analyzed using laser scanning confocal microscopy. As seen in Fig. 4*A*, the G37R or G93A Cu,Zn-SOD transfectants displayed less reactivity to phalloidin than did the mock or wild-type transfectant controls. Such lower reactivity was evident not only in the dendritic processes but also in the cell surface (Fig. 4*A*). This evidence indicates that a decrease in actin polymerization occurred in the mutated Cu,Zn-SOD transfectants. Because tubulin governs the location of the cytoplasm, we next stained the cells with an anti-α-tubulin antibody. As shown in Fig. 4*B*, there were not clarified changes among mock, wild-type, and mutated Cu,Zn-SOD transfectants in α-tubulin immunoreactivities, but some cells with two nuclei were observed in the G93A and G37R Cu,Zn-SOD transfectants. The cells were stained with propidium iodide to determine the area of the nucleus. Fig. 5 indicates the size of the nucleus per cell in each of the transfectants. The mean values of the size of mutant transfectants were almost twice those of wild-type Cu,Zn-SOD or mock transfectants, suggesting that M-phase arrest can occur in mutant-transfected cells.

One of the mutated Cu,Zn-SOD-associated proteins is actin. To examine the changes in cellular protein in the mutant transfectants, 2-D gel electrophoresis was performed. As shown in Fig. 6*A*, significant differences were not found between the wild-type and mutant Cu,Zn-SOD transfectants when a whole cell lysate was examined. However, when the cell lysate was immunoprecipitated with an anti-Cu,Zn-SOD antibody and subjected to 2-D gel electrophoretic analysis, several protein spots with molecular mass of ~40 kDa were found only in mutated Cu,Zn-SOD transfectants as shown in Fig. 6*B*. Because the molecular mass of actin is ~43 kDa, we assumed that one of the spots might be actin. To identify the spots, similarly prepared gels were subjected to Western blot analysis using an anti-actin antibody. Actin-positive spots were observed in the G37R and G93A transfectants but not in the wild-type transfectants (Fig. 7*A*). The samples were next immunoprecipitated with an anti-actin antibody and subjected to Western blot analysis using an anti-Cu,Zn-SOD antibody, the reverse of the former experiment. As shown in Fig. 7*B*, stronger signals were detected in the G37R and G93A Cu,Zn-SOD transfectants than in the wild-type transfectants. These

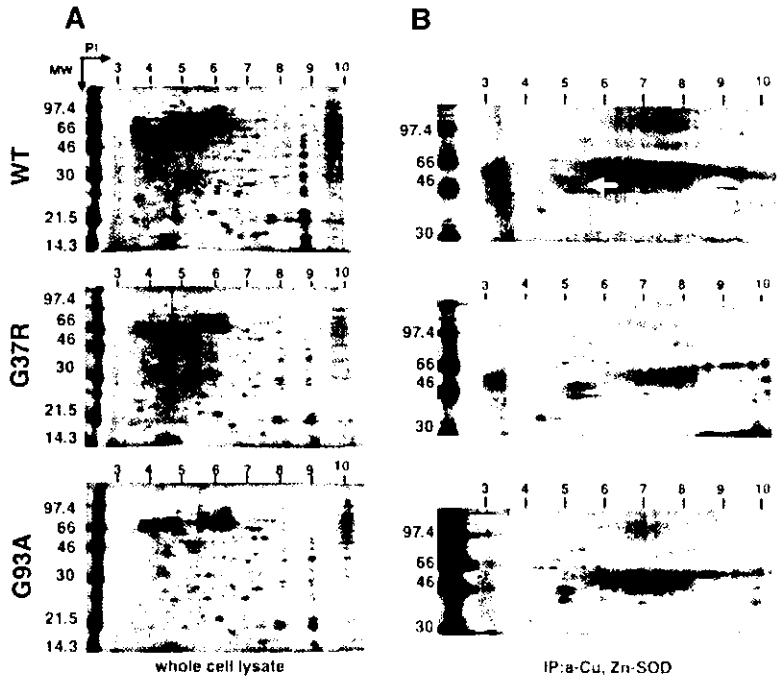

Fig. 6. Two-dimensional (2-D) gel electrophoretic pattern of wild-type and mutated Cu,Zn-SOD-transfected N2a cells. *A*: whole cell lysates (50 μg) of wild-type, G37R, and G93A Cu,Zn-SOD transfectants were subjected to 2-D gel electrophoresis and silver staining. *B*: samples were immunoprecipitated with an anti-Cu,Zn-SOD antibody and subjected to 2-D gel electrophoresis and silver staining.

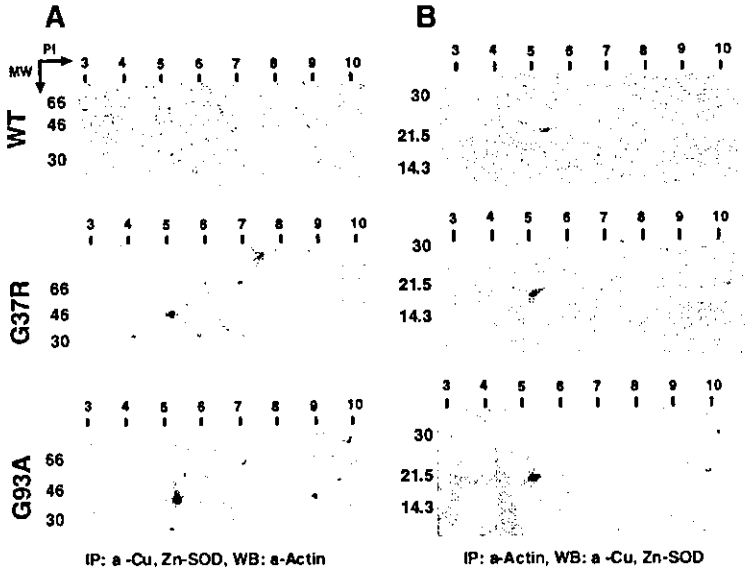

Fig. 7. Determination of Cu,Zn-SOD associated proteins. *A*: samples were immunoprecipitated with an anti-Cu,Zn-SOD antibody and subjected to 2-D gel electrophoresis (10%) and Western blot analysis using an anti-actin antibody. *B*: samples were immunoprecipitated with an anti-actin antibody and subjected to 2-D gel electrophoresis (15%) and Western blot analysis using an anti-Cu,Zn-SOD antibody.

results suggest that mutated Cu,Zn-SOD has a greater tendency to associate with actin protein.

Mutated Cu,Zn-SOD directly associate with actin in vitro. To determine whether mutated Cu,Zn-SOD directly suppressed actin polymerization, we purified wild-type and mutated Cu,Zn-SOD in a baculovirus insect cell system and performed an actin polymerization assay. In this assay, we found that both wild-type and mutated Cu,Zn-SOD did not prevent actin polymerization (data not shown). We then performed in vitro incubation of actin and Cu,Zn-SOD. Actin samples incubated with purified wild-type and mutated Cu,Zn-SOD were immunoprecipitated with anti-Cu,Zn-SOD antibody and subjected to Western blot analysis using an anti-actin antibody. As shown in Fig. 8, a band corresponding to the molecular mass of actin was observed in the mixture with the mutated Cu,Zn-SOD. These results suggest that mutated Cu,Zn-SOD directly associates with actin.

DISCUSSION

Cell cycle changes in mouse neuroblastoma N2a cells transfected with FALS-associated mutants of Cu,Zn-SOD were examined. When G37R and G93A Cu,Zn-SOD mutants were transfected into N2a cells, G_2/M arrest and significant cell growth retardation were observed. Although there were no significant changes in tubulin immunoreactivities, the mutated Cu,Zn-SOD transfectants displayed less reactivity to phalloidin than did the wild-type transfectants, indicating that actin disruption occurred in the mutant transfectants. Immunoprecipitation and 2-D gel electrophoresis followed by Western blot analysis indicated that the mutated Cu,Zn-SOD tended to associate with actin. The in vitro study in which purified Cu,Zn-SOD was incubated with actin indicated that the mutated Cu,Zn-SOD directly associated with actin. G_2/M arrest also occurred in mutated Cu,Zn-SOD-transfected NIH-3T3 cells, although the extent was much less than observed in transfectants of N2a cells (data not shown). Therefore, these phenomena are not considered to be N2a cell specific.

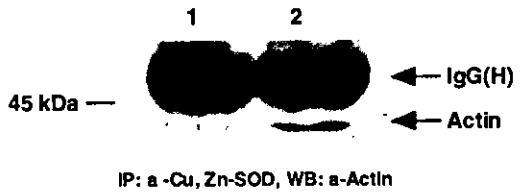

Fig. 8. In vitro association of G93A Cu,Zn-SOD with actin. After wild-type or G93A mutation, Cu,Zn-SOD (0.1 μg) was incubated with human platelet actin (0.1 μg) in actin polymerization buffer (in mM: 50 KCl, 2 $MgCl_2$, and 1 ATP) for 1 h at 24°C, and the samples were immunoprecipitated with an anti-Cu,Zn-SOD antibody and subjected to Western blot analysis using anti-actin antibody. *Lane 1*: wild-type Cu,Zn-SOD incubated with actin; *lane 2*: G93A-mutated Cu,Zn-SOD incubated with actin.

Mutated Cu,Zn-SOD have several enhanced activities that could be capable of selectively damaging interacting proteins or their associated organelles (5, 24, 36, 38). Investigators at our laboratory previously reported that Cu-binding affinities are decreased in mutated Cu,Zn-SOD (26) and mutated Cu,Zn-SOD are highly susceptible to nonenzymatic glycosylation, i.e., glycation (34). It is possible that actin-bound mutated Cu,Zn-SOD is glycated in vivo and reactive oxygen species could be produced via the Fenton reaction involving free Cu ions released from Cu,Zn-SOD (27). Recent reports indicate that hydrogen peroxide causes an increase in F- and G-actin oxidation and a decrease in the F-actin fraction (3, 4). The association of mutated Cu,Zn-SOD with actin might be unexpectedly toxic to the actin cytoskeleton.

Cytoskeletal changes and subsequent G_2/M arrest are commonly seen in apoptotic cells. However, when we performed the apoptotic assay by examining the DNA ladder, no significant apoptotic evidence was seen in mutated Cu,Zn-SOD-transfected N2a cells after 2-day serum starvation (data not shown).

The cytoskeletal changes observed in the mutated Cu,Zn-SOD in this study could be related to neuronal cell death observed in patients with FALS. In recent studies, researchers have reported that cytoskeletal proteins are significantly altered in ALS spinal motor neurons. For example, neurofilament

aggregation is known to be an early pathological hallmark of the disease process. Furthermore, Vukosavic et al. (35) reported that the level of β-actin decreases in the mutated Cu,Zn-SOD transgenic mice. The association of mutated Cu,Zn-SOD with actin reported in the present study could be an another important factor in cytoskeletal disruption and the apoptosis of neuronal cells in FALS.

The association of mutant Cu,Zn-SOD with actin could also be involved in the formation of aggregates that are observed in ALS. An increasing number of studies have stressed the role of mutant Cu,Zn-SOD-derived aggregation in the pathogenesis of ALS. Intracellular Cu,Zn-SOD aggregates are found in cultured motor neurons after the microinjection of mutant *Sod1* cDNA (11). Aggregates containing Cu,Zn-SOD were also detected in motor neurons and astrocytes of transgenic mice that expressed mutant *Sod1* (7). Mutant Cu,Zn-SOD aggregation into insoluble protein complexes is considered to be an early event in the pathogenic mechanism of FALS (18). Transfection studies indicated that mutant but not wild-type Cu,Zn-SOD forms cytoplasmic aggregates (18, 20). Such aggregates might interact inappropriately with other cellular components to impair cellular function. Pasinelli et al. (28) recently reported that mutant Cu,Zn-SOD-containing aggregates binds to Bcl-2 in spinal cord mitochondria, suggesting possible mechanisms of neurotoxicity of mutant Cu,Zn-SOD. Aggregates observed in ALS are also likely substrates for dynein-mediated transport and cause the disruption of microtubule-dependent axonal transport of other substrates. In addition, they are considered to stimulate neurodegeneration by overwhelming the capacity of the protein-folding chaperones and normal proteasome function. Thus the toxicity of mutant Cu,Zn-SOD could result from their propensity to aggregate. Similar mechanisms have been proposed for other degenerative diseases such as Alzheimer's disease, light-chain amyloidosis, and the spongiform encephalopathies (8). What, then, is the cause of the formation of such toxic aggregations? One possible mechanism is aberrant protein-protein interactions as demonstrated in mutant proteins in some neurodegenerative and/or neuromuscular disorders (9, 23). Kunst et al. (21) reported that G85R and G93A Cu,Zn-SOD bind to translocon-associated protein-δ (TRAP-δ) and lysyl-tRNA synthetase (KARS) using a yeast two-hybrid system. Although we were not able to identify TRAP-δ and KARS as proteins that bind to mutated Cu,Zn-SOD, it is possible that they were also present in the 2-D gels shown in Fig. 6. The mechanisms by which the mutated Cu,Zn-SOD associated with actin are currently under investigation. We assume that the structural changes or instability of Cu,Zn-SOD caused by the mutation suggested by the crystal structures (16) might be involved in this phenomenon. Further analysis of mutated Cu,Zn-SOD proteins will provide clues to their aberrant interactions with other proteins, including actin.

ACKNOWLEDGMENTS

We thank Dr. Yoshitaka Ikeda for technical support and critical discussion.

GRANTS

This work was supported by a grant from the Amyotrophic Lateral Sclerosis Association, a grant on Specific Diseases (Itoyama) from Ministry of Health and Welfare, Japan, the 21st Century COE Program of the Ministry of Education, Science, Culture, Sports, and Technology, and a Grant-in-Aid for Scientific Research (C) No. 15500237.

REFERENCES

1. **Andersen PM, Morita M, and Brown RH Jr.** *Genetics of Amyotrophic Lateral Sclerosis: An Overview*. London: World Federation of Neurology, Committee on Motor Neuron Disease, 1999.
2. **Arai K, Maguchi S, Fujii S, Ishibashi H, Oikawa K, and Taniguchi N.** Glycation and inactivation of human Cu-Zn-superoxide dismutase: identification of the in vitro glycated sites. *J Biol Chem* 262: 16969–16972, 1987.
3. **Banan A, Fitzpatrick L, Zhang Y, and Keshavarzian A.** OPC-compounds prevent oxidant-induced carbonylation and depolymerization of the F-actin cytoskeleton and intestinal barrier hyperpermeability. *Free Radic Biol Med* 30: 287–298, 2001.
4. **Banan A, Zhang Y, Losurdo J, and Keshavarzian A.** Carbonylation and disassembly of the F-actin cytoskeleton in oxidant induced barrier dysfunction and its prevention by epidermal growth factor and transforming growth factor alpha in a human colonic cell line. *Gut* 46: 830–837, 2000.
5. **Beckman JS, Carson M, Smith CD, and Koppenol WH.** ALS, SOD and peroxynitrite. *Nature* 364: 584, 1993.
6. **Bruijn LI, Becher MW, Lee MK, Anderson KL, Jenkins NA, Copeland NG, Sisodia SS, Rothstein JD, Borchelt DR, Price DL, and Cleveland DW.** ALS-linked SOD1 mutant G85R mediates damage to astrocytes and promotes rapidly progressive disease with SOD1-containing inclusions. *Neuron* 18: 327–338, 1997.
7. **Bruijn LI, Houseweart MK, Kato S, Anderson KL, Anderson SD, Ohama E, Reaume AG, Scott RW, and Cleveland DW.** Aggregation and motor neuron toxicity of an ALS-linked SOD1 mutant independent from wild-type SOD1. *Science* 281: 1851–1854, 1998.
8. **Bucciantini M, Giannoni E, Chiti F, Baroni F, Formigli L, Zurdo J, Taddei N, Ramponi G, Dobson CM, and Stefani M.** Inherent toxicity of aggregates implies a common mechanism for protein misfolding diseases. *Nature* 416: 507–511, 2002.
9. **Burke JR, Enghild JJ, Martin ME, Jou YS, Myers RM, Roses AD, Vance JM, and Strittmatter WJ.** Huntingtin and DRPLA proteins selectively interact with the enzyme GAPDH. *Nat Med* 2: 347–350, 1996.
10. **Cleveland DW and Rothstein JD.** From Charcot to Lou Gehrig: deciphering selective motor neuron death in ALS. *Nat Rev Neurosci* 2: 806–819, 2001.
11. **Durham HD, Roy J, Dong L, and Figlewicz DA.** Aggregation of mutant Cu/Zn superoxide dismutase proteins in a culture model of ALS. *J Neuropathol Exp Neurol* 56: 523–530, 1997.
12. **Farah CA, Nguyen MD, Julien JP, and Leclerc N.** Altered levels and distribution of microtubule-associated proteins before disease onset in a mouse model of amyotrophic lateral sclerosis. *J Neurochem* 84: 77–86, 2003.
13. **Ferrante RJ, Browne SE, Shinobu LA, Bowling AC, Baik MJ, MacGarvey U, Kowall NW, Brown RH Jr, and Beal MF.** Evidence of increased oxidative damage in both sporadic and familial amyotrophic lateral sclerosis. *J Neurochem* 69: 2064–2074, 1997.
14. **Fujii J, Myint T, Seo HG, Kayanoki Y, Ikeda Y, and Taniguchi N.** Characterization of wild-type and amyotrophic lateral sclerosis-related mutant Cu,Zn-superoxide dismutases overproduced in baculovirus-infected insect cells. *J Neurochem* 64: 1456–1461, 1995.
15. **Gurney ME, Pu H, Chiu AY, Dal Canto MC, Polchow CY, Alexander DD, Caliendo J, Hentati A, Kwon YW, Deng HX, Chen W, Zhai P, Sufit RL, and Siddique T.** Motor neuron degeneration in mice that express a human Cu,Zn superoxide dismutase mutation. *Science* 264: 1772–1775, 1994.
16. **Hart PJ, Liu H, Pellegrini M, Nersissian AM, Gralla EB, Valentine JS, and Eisenberg D.** Subunit asymmetry in the three-dimensional structure of a human CuZnSOD mutant found in familial amyotrophic lateral sclerosis. *Protein Sci* 7: 545–555, 1998.
17. **Hirano A, Nakano I, Kurland LT, Mulder DW, Holley PW, and Saccomanno G.** Fine structural study of neurofibrillary changes in a family with amyotrophic lateral sclerosis. *J Neuropathol Exp Neurol* 43: 471–480, 1984.
18. **Johnston JA, Dalton MJ, Gurney ME, and Kopito RR.** Formation of high molecular weight complexes of mutant Cu, Zn-superoxide dismutase in a mouse model for familial amyotrophic lateral sclerosis. *Proc Natl Acad Sci USA* 97: 12571–12576, 2000.
19. **Julien JP.** Amyotrophic lateral sclerosis: unfolding the toxicity of the misfolded. *Cell* 104: 581–591, 2001.
20. **Koide T, Igarashi S, Kikugawa K, Nakano R, Inuzuka T, Yamada M, Takahashi H, and Tsuji S.** Formation of granular cytoplasmic aggregates

in COS7 cells expressing mutant Cu/Zn superoxide dismutase associated with familial amyotrophic lateral sclerosis. *Neurosci Lett* 257: 29–32, 1998.

21. **Kunst CB, Mezey E, Brownstein MJ, and Patterson D.** Mutations in SOD1 associated with amyotrophic lateral sclerosis cause novel protein interactions. *Nat Genet* 15: 91–94, 1997.
22. **Lee PJ, Alam J, Wiegand GW, and Choi AM.** Overexpression of heme oxygenase-1 in human pulmonary epithelial cells results in cell growth arrest and increased resistance to hyperoxia. *Proc Natl Acad Sci USA* 93: 10393–10398, 1996.
23. **Li XJ, Li SH, Sharp AH, and Nucifora FC Jr, Schilling G, Lanahan A, Worley P, Snyder SH, and Ross CA.** A huntingtin-associated protein enriched in brain with implications for pathology. *Nature* 378: 398–402, 1995.
24. **Mourelatos Z, Gonatas NK, Stieber A, Gurney ME, and Dal Canto MC.** The Golgi apparatus of spinal cord motor neurons in transgenic mice expressing mutant Cu,Zn superoxide dismutase becomes fragmented in early, preclinical stages of the disease. *Proc Natl Acad Sci USA* 93: 5472–5477, 1996.
25. **Nguyen MD, Boudreau M, Kriz J, Couillard-Després S, Kaplan DR, and Julien JP.** Cell cycle regulators in the neuronal death pathway of amyotrophic lateral sclerosis caused by mutant superoxide dismutase 1. *J Neurosci* 23: 2131–2140, 2003.
26. **Okado-Matsumoto A, Myint T, Fujii J, and Taniguchi N.** Gain in functions of mutant Cu,Zn-superoxide dismutases as a causative factor in familial amyotrophic lateral sclerosis: less reactive oxidant formation but high spontaneous aggregation and precipitation. *Free Radic Res* 33: 65–73, 2000.
27. **Ookawara T, Kawamura N, Kitagawa Y, and Taniguchi N.** Site-specific and random fragmentation of Cu,Zn-superoxide dismutase by glycation reaction: Implication of reactive oxygen species. *J Biol Chem* 267: 18505–18510, 1992.
28. **Pasinelli P, Belford ME, Lennon N, Bacskai BJ, Hyman BT, Trotti D, and Brown RH Jr.** Amyotrophic lateral sclerosis-associated SOD1 mutant proteins bind and aggregate with Bcl-2 in spinal cord mitochondria. *Neuron* 43: 19–30, 2004.
29. **Rakhit R, Cunningham P, Furtos-Matei A, Dahan S, Qi XF, Crow JP, Cashman NR, Kondejewski LH, and Chakrabartty A.** Oxidation-induced misfolding and aggregation of superoxide dismutase and its implications for amyotrophic lateral sclerosis. *J Biol Chem* 277: 47551–47556, 2002.
30. **Rosen DR, Siddique T, Patterson D, Figlewicz DA, Sapp P, Hentati A, Donaldson D, Goto J, O'Regan JP, Deng HX, Rahmani Z, Krizus A, McKenna-Yasek D, Cayabyab A, Gaston SM, Berger R, Tanzi RE, Halperin JJ, Herzfeldt B, van den Bergh R, Hung WY, Bird T, Deng G, Mulder DW, Smyth C, Laing NG, Soriano E, Pericak-Vance MA, Haine J, Rouleau GA, Gusella JS, Horritz HR, and Brown RH Jr.** Mutations in Cu/Zn superoxide dismutase gene are associated with familial amyotrophic lateral sclerosis. *Nature* 362: 59–62, 1993.
31. **Rouleau GA, Clark AW, Rooke K, Pramatarova A, Krizus A, Suchowersky O, Julien JP, and Figlewicz D.** SOD1 mutation is associated with accumulation of neurofilaments in amyotrophic lateral sclerosis. *Ann Neurol* 39: 128–131, 1996.
32. **Sato Y, Takahashi M, Shibukawa Y, Jain SK, Hamaoka R, Miyagawa J, Yaginuma Y, Honke K, Ishikawa M, and Taniguchi N.** Overexpression of N-acetylglucosaminyltransferase III enhances the epidermal growth factor-induced phosphorylation of ERK in HeLaS3 cells by up-regulation of the internalization rate of the receptors. *J Biol Chem* 276: 11956–11962, 2001.
33. **Suzuki T, Oishi M, Marshak DR, Czernik AJ, Nairn AC, and Greengard P.** Cell cycle-dependent regulation of the phosphorylation and metabolism of the Alzheimer amyloid precursor protein. *EMBO J* 13: 1114–1122, 1994.
34. **Takamiya R, Takahashi M, Myint T, Park YS, Miyazawa N, Endo T, Fujiwara N, Sakiyama H, Misonou Y, Miyamoto Y, Fujii J, and Taniguchi N.** Glycation proceeds faster in mutated Cu, Zn-superoxide dismutases related to familial amyotrophic lateral sclerosis. *FASEB J* 17: 938–940, 2003.
35. **Vukosavic S, Stefanis L, Jackson-Lewis V, Guégan C, Romero N, Chen C, Dubois-Dauphin M, and Przedborski S.** Delaying caspase activation by Bcl-2: A clue to disease retardation in a transgenic mouse model of amyotrophic lateral sclerosis. *J Neurosci* 20: 9119–9125, 2000.
36. **Wiedau-Pazos M, Goto JJ, Rabizadeh S, Gralla EB, Roe JA, Lee MK, Valentine JS, and Bredesen DE.** Altered reactivity of superoxide dismutase in familial amyotrophic lateral sclerosis. *Science* 271: 515–518, 1996.
37. **Williamson TL and Cleveland DW.** Slowing of axonal transport is a very early event in the toxicity of ALS-linked SOD1 mutants to motor neurons. *Nat Neurosci* 2: 50–56, 1999.
38. **Yim MB, Kang JH, Yim HS, Kwak HS, Chock PB, and Stadtman ER.** A gain-of-function of an amyotrophic lateral sclerosis-associated Cu,Zn-superoxide dismutase mutant: An enhancement of free radical formation due to a decrease in Km for hydrogen peroxide. *Proc Natl Acad Sci USA* 93: 5709–5714, 1996.

Anxiolytic Effect of Hepatocyte Growth Factor Infused into Rat Brain
Koichi Isogawa; Jotaro Akiyoshi; Kensuke Kodama; Hirotaka Matsushita; Takashi...
Neuropsychobiology; 2005; 51, 1; ProQuest Medical Library
pg. 34

Original Paper

Neuropsychobiology

Neuropsychobiology 2005;51:34–38
DOI: 10.1159/000082853

Published online: December 20, 2004

Anxiolytic Effect of Hepatocyte Growth Factor Infused into Rat Brain

Koichi Isogawa[a] Jotaro Akiyoshi[a] Kensuke Kodama[a] Hirotaka Matsushita[a]
Takashi Tsutsumi[a] Hiroshi Funakoshi[b] Toshikazu Nakamura[b]

[a]Department of Neuropsychiatry, Oita University Faculty of Medicine, Oita, and [b]Division of Biochemistry, Department of Oncology, Biomedical Research Center, Osaka University Medical School, Osaka, Japan

Key Words
Anxiety · Hepatocyte growth factor · Rat

Abstract
Background: Hepatocyte growth factor (HGF) has the capacity to selectively direct thalamocortical projections into an intermediate target, the pallidum, and eventually to their final cortical destination. HGF may have a role in the mediation of anxiety. Very little is known about other central behavioral effects of HGF. ***Objective:*** Our aim was to determine what effect HGF has on anxiety in rats. ***Methods:*** HGF was infused at a constant rate into cerebral lateral ventricles and its effect on anxiety in rats was monitored. ***Results:*** In the elevated plus maze test and the black and white box test, HGF administration caused all indicators of anxiety to increase. No significant effect on general locomotor activity was seen. ***Conclusion:*** HGF infusion into the brain produces an anxiolytic effect.

Copyright © 2005 S. Karger AG, Basel

Introduction

Hepatocyte growth factor (HGF) is a potent angiogenic growth factor [1–3]. Recently, it has been reported that HGF is induced in neurons during ischemia [4] and that HGF is neuroprotective against postischemic delayed neuronal death in the hippocampus [5, 6].

In the brain, HGF is expressed by specific classes of neurons in addition to nonneuronal cells in the ependyma and choroid plexus [7]. In contrast to HGF, c-Met transcripts have been predominantly localized in neurons of the cerebral cortex, hippocampus and septum [8–10]. HGF elevated the proto-oncogene c-*fos* mRNA in cultured septal neurons, showing a functional interaction between c-Met and its ligand [10]. This result, together with the presence of c-Met in the developing brain, raised the possibility that HGF may have a neurotrophic activity on central neurons. In keeping with this hypothesis, Hamanoue et al. [11] showed that HGF promoted the survival of cultured mesencephalic tyrosine hydroxylase-positive neurons. HGF acts on calbindin-D-containing hippocampal neurons and increases their neurite outgrowth, suggesting that HGF plays an important role in the maturation and function of hippocampal neurons [12]. Transfection of HGF gene into the subarachnoid space prevent-

KARGER
Fax + 41 61 306 12 34
E-Mail karger@karger.ch
www.karger.com

© 2005 S. Karger AG, Basel
0302–282X/05/0511–0034$22.00/0

Accessible online at:
www.karger.com/nps

Jotaro Akiyoshi
Department of Neuropsychiatry
Oita University Faculty of Medicine
Hasama-Machi, Oita 879-5593 (Japan)
Tel. +81 97 586 5823, Fax +81 97 549 3583, E-Mail akiyoshi@m.ed.oita-u.ac.jp

Reproduced with permission of the copyright owner. Further reproduction prohibited without permission.

ed delayed neuronal death, accompanied by a significant increase in HGF in the cerebrospinal fluid (CSF). Prevention of delayed neuronal death by HGF is due to the inhibition of apoptosis through the blockade of bax translocation from the cytoplasm to the nucleus. HGF gene transfer into the subarachnoid space may provide a new therapeutic strategy for cerebrovascular disease [13].

HGF has the capacity to selectively direct thalamocortical projections into an intermediate target, the pallidum, and eventually to their final cortical destination [14]. Mice with a targeted mutation of the gene encoding urokinase plasminogen activator receptor (uPAR), a key component in HGF/scatter factor (SF) activation and function, have decreased levels of HGF/SF and a 50% reduction in neocortical GABAergic interneurons at embryonic and perinatal ages. Mice of the uPAR –/– strain survive until adulthood, and behavior testing demonstrates that they have an increased anxiety state [14]. HGF may have a role in the mediation of anxiety.

This is the first report to determine what effect HGF infused into cerebral lateral ventricles has on anxiety in rats.

Materials and Methods

Animals

Five-week-old male Wistar rats (Seack Yoshitomi Co., Fukuoka, Japan) were used for the present study. The number of rats was each 10 rats for experimental and control groups. The rats were housed in pairs for 3 weeks prior to the start of behavioral experiments in a sound-proof room at 24 ± 0.5°C, 50 ± 5% relative humidity, with controlled 12-hour light-dark cycles (light from 18:00 to 6:00), and were allowed free access to food and water. The room was cleaned at random in a dim, red light. All testing was performed in July during the dark phase using a dim, red light. Animal care was in accordance with the guidelines for animal experimentation of Oita Medical University.

Surgical Procedures

Each rat was anesthetized with chloral hydrate (400 mg/kg, i.p.), a brain infusion cannula (brain infusion kit, model 1007D, Alzet Corp., Palo Alto, Calif., USA) was stereotactically implanted into the lateral cerebral ventricle (0.92 mm caudal and 1.6 mm lateral to the bregma and 3.5 mm deep), and a mini-osmotic pump (micro-osmotic pump, model 1003D; Alzet Corp.) was placed into subcutaneous tissue of the back. After the operation, rats were injected with ceftriaxone sodium (20 mg/kg, i.p.). Either HGF (30 μg) in the experimental group or a vehicle in the control group (Ringer's solution, pH = 7.4) was infused at a constant rate into the lateral ventricle of the rat via the micro-osmotic pump over a 3-day period. Tsuzuki et al. [15] reported that continuous intraventricular administration of the human recombinant HGF by using an osmotic mini-pump reduced the infarct volumes in the brain lesion and prevented apoptotic neuronal cell death.

Materials

A vehicle (Ringer's isotonic solution, pH 7.4) was used as a control. HGF was synthesized in the Division of Biochemistry, Department of Oncology, Biomedical Research Center, Osaka University Medical School.

Behavioral Testing

The first day of testing was concerned with measuring anxiety. All rats were subjected to the 'elevated plus maze', followed on the same day by the 'black and white box' test. Ethological measures in elevated plus maze comprised frequency scores for supported head dipping (exploratory movement of head/shoulders over the side of the maze), and stretched attend posture (exploratory posture in which the body is stretched forward then retracted to the original position without any forward locomotion). At the end of the day, rats received inescapable electric foot shocks to condition fear. On the second day, rats performed the conditioned fear test. Conditioned response models of fear and anxiety are based on classical procedures of fear conditioning [16]. On day 1 of fear conditioning, each rat was individually subjected to 5 min of inescapable electric foot shock (10 shocks of 1 s duration and 2 mA intensity, each shock separated by an interval of 40 s) in a chamber with a grid floor (31 × 30 × 25 cm). Twenty-four hours after the foot shock, the rats were again placed in the shock chamber and observed for 5 min without shocks. During the 5-min observation period, freezing behavior was recorded using a video camera. Every 10 s, the behavior was classified as either freezing or active. Freezing was defined as the absence of any observable movement of the body and/or vibrissae, aside from the movement necessitated by respiration. We also investigated general locomotor activity.

Elevated Plus Maze

The elevated plus maze consisted of two opposite open arms (50 × 10 cm) without side walls and two opposite enclosed arms (50 × 8 × 40 cm), and was elevated 50 cm above the floor. The rats were placed in the middle of the maze facing one of the open arms, and immediately left alone in the test room. They were observed and their responses were recorded for 300 s via a video camera. Five parameters were measured during 5 min: (1) time spent in the open arms, (2) total number of entries into the open arms, (3) number of stretched attend postures, and (4) number of head dips over the edge of the platform.

Black and White Box

The wall of the test box was 27 cm high, the size of each compartment was 23 × 27 cm, and the two compartments were connected by a 10-cm high semicircular hole. Both white and red light sources were 40 W, and the light sources were located 17 cm above the floor of the two compartments. The rats were placed in the center of the white compartment and the number of entries and time spent in the black and white compartments during 5 min were recorded. An entry into another compartment was scored whenever a rat placed all four paws in that compartment.

General Locomotor Activity

We investigated general locomotor activity of the rats by means of infrared photobeam breaks, since locomotion influences exploratory activity. The apparatus was 36 cm in height and the floor size was 30 × 30 cm. We measured the locomotor activity by photobeam breaks for 2 h.

Reproduced with permission of the copyright owner. Further reproduction prohibited without permission.

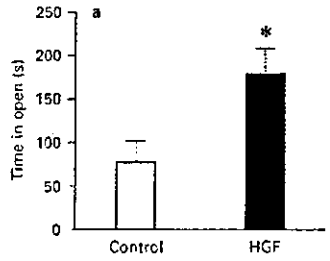

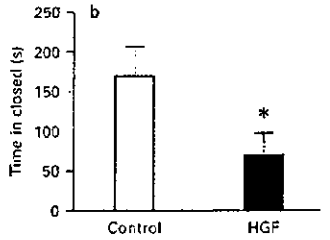

Fig. 1. a Time spent in the open arm of the elevated plus maze was significantly increased in the HGF-infused group compared to the control group. **b** Time spent in the closed arm of the elevated plus maze was significantly decreased in the HGF-infused group compared to the control group. * $p < 0.05$ vs. vehicle- and HGF-infused group.

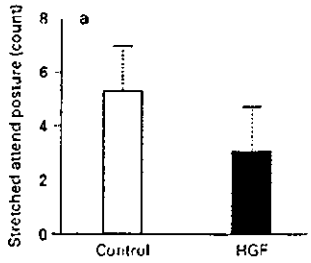

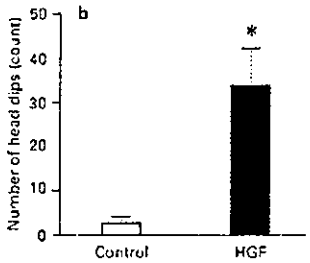

Fig. 2. a No effect of HGF or the control vehicle on the number of stretched attend postures in the elevated plus maze was seen. **b** The number of head dips in the elevated plus maze was significantly increased in the HGF-infused group compared to the control group. * $p < 0.05$ vs. vehicle- and HGF-infused group.

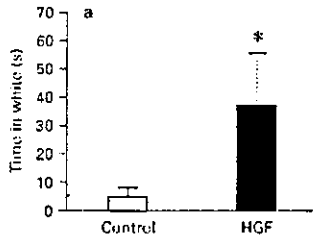

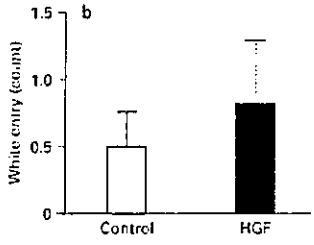

Fig. 3. In the black and white box test, the time spent in the white chamber was significantly increased in the HGF-infused group, compared to the controls (**a**). **b** No significant effect of HGF on the number of white chamber entries was seen. * $p < 0.05$ vs. vehicle- and HGF-infused group.

Statistical Analysis

The data were presented as means ± SE of the individual values from each group. Behavioral data (except for general locomotor activity) were analyzed using the Student t test for independent samples. The data of general locomotor activity were subjected to a two-way ANOVA. Statistical significance was accepted for $p < 0.05$.

Results

Time spent in the open arm of the elevated plus maze was significantly increased in the HGF-infused group, compared to the vehicle-treated group [$t(18) = 2.43$, $p < 0.031$; fig. 1a]. Time spent in the closed arm of the elevated plus maze was significantly decreased in the HGF-infused group compared to the control group [$t(18) = 2.23$, $p < 0.045$; fig. 1b]. No effect of HGF or the control vehicle on the number of stretched attend postures in the elevated plus maze was seen [$t(18) = 1.01$; fig. 2a]. The number of head dips in the elevated plus maze was significantly increased in the HGF-infused group compared to the control group. The number of head dips was significantly increased in the HGF-infused group compared to the vehicle-treated group [$t(18) = 2.61$, $p < 0.023$; fig. 2b]. In the black and white box test, the time spent in the white chamber was significantly decreased in the HGF-infused group, compared to the controls [$t(18) = 2.25$, $p < 0.048$; fig. 3a]. No significant effect of HGF on the number of white chamber entries was seen [$t(18) = 0.65$; fig. 3b]. The amount of conditioned fear stress-induced freezing behavior was significantly decreased in the HGF-infused group compared to the vehicle-treated group [$t(18) = 2.38$, $p < 0.036$; fig. 4]. No significant differences between the two groups were seen in general locomotor activity ($F_{2,35} = 1.30$; fig. 5).

Reproduced with permission of the copyright owner. Further reproduction prohibited without permission.

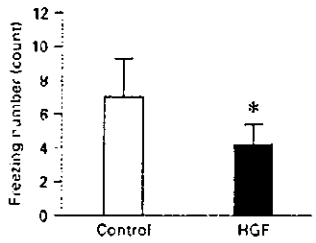

Fig. 4. Level of freezing induced by conditioned fear was significantly decreased in the HGF-infused group, compared to the controls. * $p < 0.05$ vs. vehicle- and HGF-infused group.

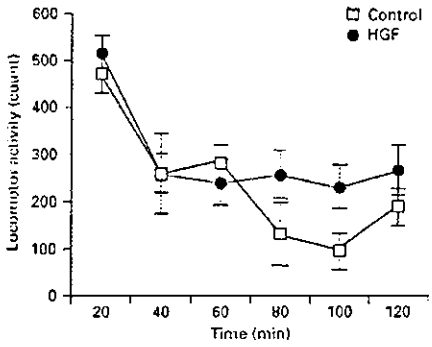

Fig. 5. No significant effect of HGF on general locomotor activity (number of photobeam breaks) was seen. Data are means ± SEM.

Discussion

This study provides the first evidence that HGF has an anxiolytic effect on the rat. HGF infusion into a lateral ventricle decreased anxiety as measured in the elevated plus maze and black and white box tests.

HGF was originally known as a cell mitogen and motogen, and has since been found to be a multifunctional growth factor with a variety of biological activities in numerous types of cells [17, 18]. The variety of biological functions attributed to HGF results from its interaction with its only known high-affinity transmembrane receptor, c-Met tyrosine kinase, present on target cells including central neurons [10, 19]. Coexpression of c-Met and HGF is oncogenic, and has been implicated in the progression of certain malignancies, in part, by decreasing tumor cell death and apoptosis [20, 21]. HGF and c-Met have been found to be present in specific subtypes of hippocampal neurons, cortex, septum, and cerebellum of both developing and adult mammalian brains [10, 12], but few reports exist concerning the biological activity of HGF in the CNS. A HGF-activating protease, HGF activator (HGFA), has recently been identified as a key enzyme that regulates the activity of HGF in vivo. HGFA appears to be associated with the cell surface. The HGFA antibody stained only astrocytes in the white matter in all the brain tissues. Expression of the mRNAs of HGF and HGFA was also seen in white matter astrocytes [22]. Recent studies have recognized effects of HGF on motor neuron survival, development and maturation, and on the function of cortical and hippocampal neurons in the developing brain [11, 12]. Tsuboi et al. [23] reported that consistent with the immunohistochemical data, a significantly higher concentration of HGF in Alzheimer's disease (AD) CSF was found as compared with controls. A significant correlation was also seen between CSF HGF levels and white matter high-signal foci determined on brain magnetic resonance imaging in AD patients. CSF HGF levels correspond with the white matter damage in AD brain [23].

Treatment with HGF induced an anxiolytic effect. But the mechanism of action of HGF has not been elucidated. The c-Met receptor has a heterodimeric protein which contains intracellular tyrosine kinase domains. Binding of HGF to c-Met might induce the anxiolytic effect [24]. HGF has the capacity to selectively direct thalamocortical projections into an intermediate target, the pallidum, and eventually to their final cortical destination. Mice with a targeted mutation of the gene encoding uPAR, a key component in HGF/SF activation and function, have decreased levels of HGF/SF and a 50% reduction in neocortical GABAergic interneurons at embryonic and perinatal ages. Mice of the uPAR –/– strain survive until adulthood, and behavior testing demonstrates that they have an increased anxiety state [14]. HGF may have a role in the mediation of anxiety.

In summary, this study reports that HGF infusion into the brain produced an anxiolytic effect in rats, as evaluated using the elevated plus maze, black and white box tests and conditioned fear test.

Reproduced with permission of the copyright owner. Further reproduction prohibited without permission.

References

1 Aoki M, Morishita R, Taniyama Y, Kida I, Moriguchi A, Matsumoto K, Nakamura T, Kaneda Y, Higaki J, Ogihara T: Angiogenesis induced by hepatocyte growth factor in non-infarcted myocardium and infarcted myocardium: Up-regulation of essential transcription factor for angiogenesis. Gene Ther 2000;7: 417–427.

2 Hayashi S, Morishita R, Nakamura S, Yamamoto K, Moriguchi A, Nagano T, Taizi M, Noguchi H, Matsumoto K, Nakamura T, Higaki J, Ogihara T: Potential role of hepatocyte growth factor, a novel angiogenic growth factor, in peripheral arterial disease: Down-regulation of HGF in response to hypoxia in vascular cells. Circulation 1999;100:11301–11308.

3 Morishita R, Nakamura S, Hayashi S, Taniyama Y, Moriguchi A, Nagano T, Taiji M, Noguchi H, Takeshita S, Matsumoto K, Nakamura T, Higaki J, Ogihara T: Therapeutic angiogenesis induced by human recombinant hepatocyte growth factor in rabbit hind limb ischemia model as cytokine supplement therapy. Hypertension 1999;33:1379–1384.

4 Hayashi T, Abe K, Sakurai M, Itoyama Y: Inductions of hepatocyte growth factor and its activator in rat brain with permanent middle cerebral artery occlusion. Brain Res 1998;799: 311–316.

5 Miyazawa T, Matsumoto K, Ohmichi H, Katoh H, Yamashima T, Nakamura T: Protection of hippocampal neurons from ischemia-induced delayed neuronal death by hepatocyte growth factor: A novel neurotrophic factor. J Cereb Blood Flow Metab 1998;18:345–348.

6 Yamada T, Yoshiyama Y, Tsuboi Y, Shimomura T: Astroglial expression of hepatocyte growth factor and hepatocyte growth factor activator in human brain tissues. Brain Res 1997; 762:251–255.

7 Jung W, Castrén E, Odenthal M, Vande Woude G, Dienes HP, Lindholm D, Schirmacher P: Expression and functional interaction of hepatocyte growth factor-scatter factor (HGF-SF) and its receptor c-met in mammalian brain. J Cell Biol 1994 126:485–494.

8 Achim CL, Katyal S, Wiley CA, Shiratori M, Wang G, Oshika E, Petersen BE, Li J-M, Michalopoulos GK: Expression of HGF and c-met in the developing and adult brain. Brain Res Dev Brain Res 1997;102:299–303.

9 Honda S, Kagoshima M, Wanaka A, Tohyama M, Matsumoto K, Nakamura T: Localization and functional coupling of HGF and c-met/HGF receptor in rat brain: Implication as neurotrophic factor. Brain Res Mol Brain Res 1995;32:197–210.

10 Jung W, Castren E, Odenthal M, Vande Woude GF, Ishii T, Dienes HP, Lindholm D, Schirmacher P: Expression and functional interaction of hepatocyte growth factor-scatter factor and its receptor c-met in mammalian brain. J Cell Biol 1994;126:485–494.

11 Hamanoue M, Takemoto N, Matsumoto K, Nakamura T, Nakajima K, Kohsaka S: Neurotrophic effect of hepatocyte growth factor on central nervous system neurons in vitro. J Neurosci Res 1996;43:554–564.

12 Korhonen L, Sjoholm U, Fakei N, Kern MA, Schirmacher P, Castren E, Lindholm D: Expression of c-Met in developing rat hippocampus: Evidence for HGF as a neurotrophic factor for calbindin D-expressing neurons. Eur J Neurosci 2000;12:3453–3461.

13 Hayashi K, Morishita R, Nakagami H, Yoshimura S, Hara A, Matsumoto K, Nakamura T, Kaneda Y, Ogihara T, Sakai N: Gene therapy for preventing neuronal death using hepatocyte growth factor: In vivo gene transfer of HGF to subarachnoid space prevents delayed neuronal death in gerbil hippocampal CA1 neurons. Gene Ther 2001;8:1167–1173.

14 Powell EM, Campbell DB, Stanwood GD, Davis C, Noebels JL, Levitt P: Genetic disruption of cortical interneuron development causes region- and GABA cell type-specific deficits, epilepsy, and behavioral dysfunction. J Neurosci 2003;23:622–631.

15 Tsuzuki N, Miyazawa T, Matsumoto K, Nakamura T, Shima K: Hepatocyte growth factor reduces the infarct volume after transient focal cerebral ischemia in rats. Neurol Res 2001;23: 417–424.

16 LeDoux JE: The Emotional Brain. New York, Simon and Schuster, 1996.

17 Rosen EM, Nigam SK, Goldberg ID: Scatter factor and the c-met receptor: A paradigm for mesenchymal epithelial interaction. J Cell Biol 1994;127:1783–1787.

18 Zarnegar R, Michalopoulos G: The many faces of hepatocyte growth factor: From hepatopoiesis to hematopoiesis. J Cell Biol 1995;129: 1177–1180.

19 Park M, Dean M, Kaul K, Braun MJ, Gonda MA, Vande Woude GF: Sequence of MET protooncogene cDNA has features characteristic of the tyrosine kinase family of growth-factor receptors. Proc Natl Acad Sci USA 1987;84: 6379–6383.

20 Bowers DC, Fan S, Walter K, Abounader R, Williams JA, Rosen EM, Laterra J: Scatter factor/hepatocyte growth factor activates AKT and protects against cytotoxic death in human glioblastoma via PI3-kinase and AKT-dependent pathways. Cancer Res 2000;60:4277–4283.

21 Fan S, Ma YX, Wang J, Yuan R, Meng Q, Cao Y, Laterra J, Goldberg ID, Rosen EM: The cytokine scatter factor inhibits apoptosis and enhances DNA repair by a common mechanism involving signaling through phosphatidyl inositol 3′ kinase. Oncogene 2000;19:2212–2223.

22 Yamada K, Moriguchi A, Morishita R, Aoki M, Nakamura Y, Mikami H, Oshima T, Nomiya M, Kaneda Y, Higaki J, Ogihara T: Efficient oligonucleotide delivery using the HVJ-liposome method in the central nervous system. Am J Physiol 1996;271:R1212–R1220.

23 Tsuboi Y, Kakimoto K, Nakajima M, Akatsu H, Yamamoto T, Ogawa K, Ohnishi T, Daikuhara Y, Yamada T: Increased hepatocyte growth factor level in cerebrospinal fluid in Alzheimer's disease. Acta Neurol Scand 2003; 107:81–86.

24 Furge KA, Zhang YW, Vande Woude GF: Met receptor tyrosine kinase: Enhanced signaling through adapter proteins. Oncogene 2000;19: 5582–5589.

Reproduced with permission of the copyright owner. Further reproduction prohibited without permission.

Available online at www.sciencedirect.com
SCIENCE DIRECT®
Biochemical and Biophysical Research Communications 319 (2004) 1152–1158
BBRC
www.elsevier.com/locate/ybbrc

Hepatocyte growth factor attenuates cerebral ischemia-induced learning dysfunction

Ichiro Date,[a] Norio Takagi,[a] Keiko Takagi,[a] Tomoyuki Kago,[a] Kunio Matsumoto,[b] Toshikazu Nakamura,[b] and Satoshi Takeo[a,*]

[a] *Department of Pharmacology, Tokyo University of Pharmacy and Life Science, 1432-1 Horinouchi, Hachioji, Tokyo 192-0392, Japan*
[b] *Division of Molecular Regenerative Medicine, Course of Advanced Medicine, Osaka University Graduate School of Medicine, 2-2-B7 Yamadaoka, Suita, Osaka 565-0871, Japan*

Received 11 May 2004
Available online 1 June 2004

Abstract

Hepatocyte growth factor (HGF) acts as an organotropic factor for regeneration and protection in various organs and has the ability to attenuate cerebral ischemia-induced cell death. However, the e ect of HGF on learning and memory function after a cerebral ischemic event is unknown. We demonstrate here that administration of human recombinant HGF (hrHGF) into the ventricle reduced the prolongation of the escape latency in the acquisition and retention tests in the water maze task on days 12–28 after microsphere embolism-induced cerebral ischemia. In addition, disruption of the blood–brain barrier at the early stage after microsphere embolism, which was determined by FITC–albumin leakage, was markedly reduced by treatment with hrHGF. We demonstrated that this e ect of hrHGF on the blood–brain barrier was associated with protection against the apoptotic death of the cerebral endothelial cells at the early stage after the ischemia. These results suggest that hrHGF can prevent the learning and memory dysfunction soon after sustained cerebral ischemia by protecting against injury to the endothelial cells. The use of HGF may be a potent strategy for the treatment of cerebrovascular diseases, including cerebral infarct and vascular dementia.
2004 Elsevier Inc. All rights reserved.

Keywords: Brain; Cerebral ischemia; Microsphere embolism; Learning and memory; Water maze test; Hepatocyte growth factor; Blood–brain barrier; Endothelial cells; Apoptosis; bcl family

Hepatocyte growth factor (HGF) was initially identified and cloned as a potent mitogen for hepatocytes [1,2]. The activation of the HGF receptor c-Met evokes diverse cellular responses, including mitogenic, motogenic, and morphogenic activities in various types of cells [3,4]. In addition to the physiological roles of HGF as an organotropic factor for regeneration and protection in various organs [3–6], HGF has been shown to attenuate ischemia-induced injuries under pathophysiological conditions, including cardiac ischemia/reperfusion [7] and hind limb ischemia [8,9] through anti-apoptotic and angiogenic activities. Previous studies showed that both HGF and c-Met were expressed in the brain [10,11]. Recent studies have shown that treatment with exogenous HGF prevented neuronal cell death in the hippocampal CA1 region after transient global cerebral ischemia in gerbils [12] and reduced the infarct volume after transient focal cerebral ischemia in rats [13]. Such e ects might have been mediated through the anti-apoptotic activity of HGF. However, not only the mechanisms underlying protective e ects of HGF, but also the ability of HGF to attenuate learning and memory dysfunction caused by sustained and severe cerebral ischemia, have not yet been clarified. To evaluate protective and therapeutic potencies of HGF for cerebral ischemic diseases, we examined the e ect of human recombinant HGF (hrHGF) on cerebral ischemia-induced learning and memory dysfunction and on injury of cerebral vessels. For this purpose, we used the microsphere-induced cerebral embolism model in rats. Microsphere-induced cerebral embolism

* Corresponding author. Fax: +81-426-76-5560.
E-mail address: takeos@ps.toyaku.ac.jp (S. Takeo).

0006-291X/$ - see front matter 2004 Elsevier Inc. All rights reserved.
doi:10.1016/j.bbrc.2004.05.100

induces widespread formation of small emboli and multiple infarct areas in the brain [14]. Thus, this model is considered to mimic focal ischemia-induced human stroke [15] or multi-infarct dementia [16]. Indeed, we have reported that microsphere-induced cerebral embolism induces severe learning and memory dysfunction as assessed by the water maze task, active avoidance task, and passive avoidance task [17,18].

In the present study, we demonstrated that treatment with hrHGF reduced learning and memory dysfunction in the water maze test and protected the endothelial cells against apoptotic cell death after sustained cerebral ischemia. The protection of cerebral vessel injuries may retain the integrity of blood–brain barrier after severe brain ischemia.

Materials and methods

Recombinant HGF. Human recombinant HGF (hrHGF) was purified from the culture media of Chinese hamster ovary cells transfected with an expression vector containing human HGF cDNA as described [2,19]. The purity of hrHGF was >98%, as determined by SDS-PAGE.

Microsphere embolism model. Male Wistar rats weighing 180–220 g (Charles River Japan, Atsugi, Japan) were used in the present study. The animals were maintained in a cage with a 12-h light/12-h dark cycle, at a temperature of 23 1 C, and a humidity of 55 5% throughout the experiment. The animals had free access to food and water according to the National Institute of Health Guide for the Care and Use of Laboratory Animals and the Guideline for Experimental Animal Care issued by the Prime Minister's O ce of Japan. All e orts were made to minimize the animals' su ering, to reduce the number of animals used, and to utilize alternatives to in vivo techniques, if available. The study protocol was approved by the Committee of Animal Care and Welfare of Tokyo University of Pharmacy and Life Science.

Microsphere-induced cerebral embolism was performed by the method described previously [14]. In brief, rats were anesthetized intraperitoneally with 40 mg/kg sodium pentobarbital. The right external carotid and pterygo-palatine arteries were temporarily occluded with strings. A needle connected to a polyethylene catheter (3 French, Atom, Tokyo) was inserted into the right common carotid artery. Seven hundred microspheres (47.5 0.5 μm in diameter, Perkin–Elmer Life Science), suspended in 20% dextran solution, were injected into the right internal carotid artery through the cannula. After the injection, the needle was removed, and the puncture wound was then repaired with surgical glue. Next, the strings occluding the right external carotid and pterygo-palatine arteries were released. It took 2–3 min to restart the blood flow to the brain areas supplied by the right external carotid and pterygo-palatine arteries. The rats that underwent a sham operation received the same volume of vehicle without microspheres.

Administration of human recombinant HGF. hrHGF was diluted in physiological saline and infused into the right ventricle using an osmotic pump (Alzet model 2001, Palo Alto, CA, USA) attached to a 30-gauge needle implanted 1.5 mm lateral and 0.8 mm posterior to the bregma, and at a depth of 4 mm from the cortical surface. To start infusion just after needle implantation, each osmotic pump was preincubated in physiological saline at 37 C according to the instructions for use of the Alzet. The infusion of hrHGF was begun at 10 min after the injection of microspheres at a flow rate of 1.0 μl/h and a dose of 10 or 30 μg/7 days/animal.

Neurological deficits. Fifteen hours after the operation for microsphere-induced cerebral embolism, the behavior of operated rats with or without administration of hrHGF was scored on the basis of paucity of movement, truncal curvature, and forced circling during locomotion, which are considered to be typical symptoms of stroke in rats [20,21]. The criteria described previously were used for the scoring [14]. Each item was rated from 3 to 0 (3, very severe; 2, severe; 1, moderate; and 0, little or none). Rats with a total score of 7–9 points were used in the present study.

Water maze test. The water maze test was performed according to the method described previously [18]. The acquisition test was started on day 12 after the operation. Animals were tested in the water maze by using a 3 trials/day regimen. The water maze apparatus (model TARGET/2; Neuroscience, Tokyo, Japan) consisted of a circular pool with a diameter of 170 cm, which was filled with water to a 30 cm depth. The water temperature was maintained at 23 1 C. A hidden transparent circular platform with a diameter of 12 cm was placed 1.5 cm below the surface of the water and kept in a constant position in the center of one of the four quadrants of the pool. The animals were released from three randomly assigned start locations (excluding the platform-containing quadrant). When a rat mounted the platform, it was kept there for 30 s. Data collection was automated by an online video-tracking device designed to track an object in a field. Escape latency (the time to climb onto the platform) was determined for each trial with a behavioral tracing analyzer (BAT-2; Neuroscience). The cut-o time for each trial was set at 180 s. Each trial was performed with an intertrial interval of approximately 1 h.

The retention test was performed on days 21 and 28 after the operation to determine whether the animals could retain the spatial navigation ability in the hidden platform test. The regimen and starting point used for this task were the same as those conducted in the acquisition test on day 14.

Determination of viable area. Coronal brain sections (20 μm thick) were stained with hematoxylin and eosin for determination of non-infarct areas. The observed image was incorporated into a personal computer using a scanner (EPSON TWIN PRO, Japan). Then the non-infarct area was measured as a percentage of the contralateral hemisphere using an image analysis software (NIH image 1.63, NIH, USA).

Measurements of FITC–albumin leakage area. Fluorescein isothiocyanate-conjugated albumin (FITC–albumin, Sigma, Tokyo, Japan) was injected into both carotid arteries for morphological observation of cerebral blood vessels. Injection of FITC-albumin was conducted by a modified method of Cavaglia et al. [22]. Rats on day 28 after the operation were anesthetized with an intraperitoneal injection of 40 mg/kg sodium pentobarbital (Abbott Laboratories). Bilateral carotid arteries were exposed and cannulated with a polyethylene tube (SP 31, Natume, Tokyo, Japan) attached to a 24-gauge needle. FITC-albumin solution (10 mg/ml 0.1 M phosphate-bu ered saline, pH 7.4) was perfused through the carotid arteries at a rate of 1 ml/min (10 ml/kg) using a syringe pump (CFV-2100, Nihon Kohden, Japan). To avoid elevation of systemic blood pressure, we withdrew the same amount of blood from the inferior vena cava. Immediately following perfusion, the rats were decapitated and their brains were isolated. The lag time between decapitation and immersion fixation never exceeded 2 min. Brains were fixed for 24 h in 4% paraformaldehyde and then cryoprotected in a 10%, 20%, and 30% sucrose solution for 4 h for each concentration. Thereafter, they were embedded in Tissue-Tek O.C.T. compound (O.C.T. compound, Sakura, Tokyo, Japan) and frozen in liquid nitrogen. Coronal brain sections (40 μm thick) were cut on a cryostat (Type 4559; Tissue-Tek, Sakura, Tokyo, Japan) and thaw-mounted on poly-L-lysine-coated microslide glasses (Muto Pure Chemicals, Japan). Sections were embedded in 0.1 M phosphate-buffered saline (PBS) for 30 min, mounted with DAKO Fluorescent mounting medium (DAKO, USA), and observed under a fluorescence microscope (Olympus, BX-52, Tokyo, Japan). Images were incorporated into a personal computer using Viewfinder Lite and Studio Lite software (Pixcera, Los Gatos, CA, USA). Then the area of FITC–albumin leakage regions (FITC-stained areas out of the cerebral

vessels) was measured using an image analysis software (NIH image 1.63, NIH, USA).

TUNEL-positive endothelial cells. Coronal sections (10 μm thick) were used for detection of terminal deoxynucleotidyl transferase-mediated dUTP nick end-labeling (TUNEL)-positive cells. TUNEL-positive cells were identified by using an in situ Apoptosis Detection Kit (MK500, TakaRa Bio, Siga, Japan). After having been washed, the sections were treated with 1.5% goat serum and then incubated overnight with polyclonal rabbit anti-vWF (DAKO). Subsequently, they were incubated with the biotinylated anti-rabbit IgG, and then incubated with streptavidin–biotin–peroxidase solution (Vector Laboratories). Color development was performed by using the Nova Red substrate kit. The number of TUNEL-positive endothelial cells in the right cerebral hemisphere was counted under 400 magnification (Olympus BX-52) in four sections per animal. The microscopic observations were performed by a person unaware of the study group.

Immunoblotting. Animals were sacrificed by decapitation, and their heads were quickly near-frozen in liquid nitrogen. The cerebral cortex was dissected and homogenized in the ice-cold 125 mM Tris–HCl, pH 7.4, containing 320 mM sucrose, 2 mM sodium orthovanadate, 20 mM sodium diphosphate decahydrate, 20 mM DL-α-glycerophosphate, 0.1 mM phenylmethylsulfonyl fluoride, and 5 μg/ml each of antipain, aprotinin, and leupeptin. Homogenates that had been solubilized by boiling for 5 min in SDS sample bu er (10% glycerol, 5% β-mercaptoethanol, and 2% SDS, in 62.5 mM Tris–HCl, pH 6.8) were separated on polyacrylamide gels and transferred to a polyvinylidene difluoride membrane. Protein blots were incubated with the appropriate antibodies, and the bound antibody was detected by the enhanced chemiluminescence method (Amersham Biosciences, Piscataway, NJ, USA). Quantification was performed using computerized densitometry and an image analyzer (ATTO, Tokyo, Japan). Care was taken to ensure that bands to be semiquantified were in the linear range of response. Antibodies used were anti-Bax, anti-Bcl-xL, and anti-Bcl-2 (Santa Cruz Biotechnology, Santa Cruz, CA, USA).

Statistics. The results were expressed as means SEM. Di erences between two groups were evaluated statistically by using the unpaired Student's *t* test. Statistical comparison among four groups was evaluated by ANOVA followed by Fisher's protected least significant di erence test. Di erences with a probability of 5% or less were considered significant ($p < 0.05$).

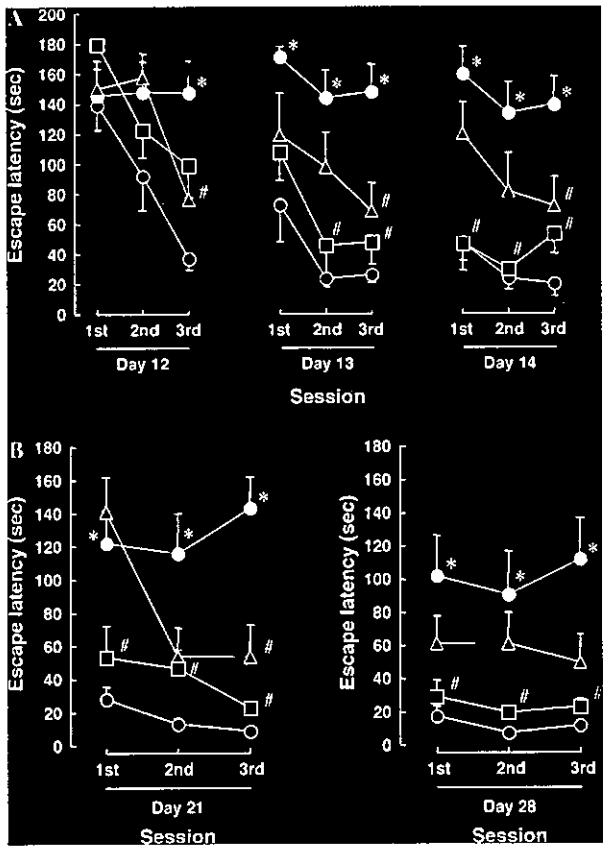

Fig. 1. Changes in the escape latency of the acquisition (A) and the retention (B) tests in the water maze task for the sham-operated (open circle), hrHGF-untreated ME (closed circle), and 10 (open triangle) or 30 (open squares) μg/7 days/animal hrHGF-treated ME rats. The escape latency was determined on days 12–14 after the operation. Each value represents the mean SEM of eight animals. The symbol * represents significant di erence from the sham-operated group ($p < 0.05$); The symbol # represents significant di erence from the hrHGF-untreated ME group ($p < 0.05$).

Results

Operation

In the present study, microspheres were injected into 86 rats. Sixty-four of the surviving rats (74.4%) showed stroke-like symptoms with a total score of 7–9 points. Seven (8.1%) and two animals (2.3%) showed the stroke-like symptoms with score of 4–6 and 2–3 points, respectively. Thirteen rats (15.1%) died before all examinations were completed.

Prolonged observations after the microsphere embolism

E ects of hrHGF on the water maze task

To determine the e ect of hrHGF on learning and memory function, we first conducted the acquisition test in the water maze task on days 12–14 after the operation (Fig. 1A). There was a significant di erence in the escape latency by groups ($F_{3,28} = 18.5$; $p < 0.0001$) and by days ($F_{8,224} = 11.9$; $p < 0.0001$). The group by day interaction was significant ($p < 0.05$). The escape latency of the sham-operated rats was shortened along with the trial number, whereas that of the ME rats was markedly prolonged compared with that of the sham-operated rats. Analysis by Fisher's PLSD test showed that the escape latency of the ME rats was significantly lengthened compared with that of the sham-operated rats from the third trial of day 12 to the third trial of day 14 ($p < 0.05$). Treatment with hrHGF dose-dependently attenuated the prolonged escape latency of the hrHGF-untreated ME rats. Treatment with 10 μg/7 days/animal hrHGF reduced the prolongation at the third trials of days 12, 13, and 14 ($p < 0.05$), whereas the prolongation of the escape latency in the 30 μg/7 days/animal hrHGF-treated rats was attenuated from the second trial of day 13 to the third trial of 14 day ($p < 0.05$). Furthermore, the retention test was performed on days 21 and 28 to determine the retention of the spatial navigation ability by using the same regimen as applied for the acquisition

test on day 14 (Fig. 1B). On day 21, there was a significant di erence in the escape latency by groups ($F_{3,28} = 14.6$; $p < 0.0001$) and by days ($F_{2,56} = 6.0$; $p < 0.0001$). The group by day interaction was significant ($p < 0.01$). On day 28, there was a significant difference in the escape latency by groups ($F_{3,28} = 9.3$; $p < 0.001$), but not by days ($F_{2,56} = 0.4$; $p = 0.7$). The group by day interaction was not significant ($p = 0.9$). Fisher's PLSD test revealed that the escape latency of the ME rat from the first to third trials in the retention test was significantly lengthened compared with that of the sham-operated rats on days 21 and 28 ($p < 0.05$; Fig. 1B). The escape latency of 30 μg/7 days/animal hrHGF-treated ME rats was significantly attenuated compared with that of the hrHGF-untreated ME rats from the first to the third trials on days 21 and 28 ($p < 0.05$; Fig. 1B).

Histological analysis

We next determined the viable area by examining coronal sections on day 28 after the operation. Microsphere embolism caused a marked decrease in the viable area of the ipsilateral hemisphere, and this decrease was dose-dependently lessened by treatment with hrHGF (Fig. 2).

Observations at the early period after the microsphere embolism

E ect of hrHGF on blood–brain barrier leakage

Brain ischemia would induce disruption of blood–brain barrier (BBB), and this disruption could initiate the development of brain injuries after ischemia. So we next examined BBB leakage after the ME by injecting

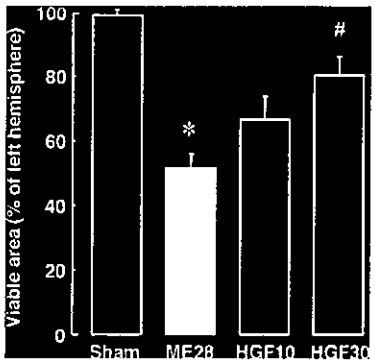

Fig. 2. E ect of hrHGF on viable areas of the sham-operated (Sham), hrHGF-untreated ME (ME28), and 10 (HGF10) or 30 (HGF30) μg/7 days/animal hrHGF-treated rats on day 28 after the operation. Viable areas were estimated by measuring hematoxylin and eosin-stained areas of brain sections. Each value represents the mean percentage of that for the corresponding contralateral hemisphere SEM ($n = 5$–8). The symbol * represents significant di erence from the sham-operated rats ($p < 0.05$); The symbol # represents significant di erence from the hrHGF-untreated ME rats ($p < 0.05$).

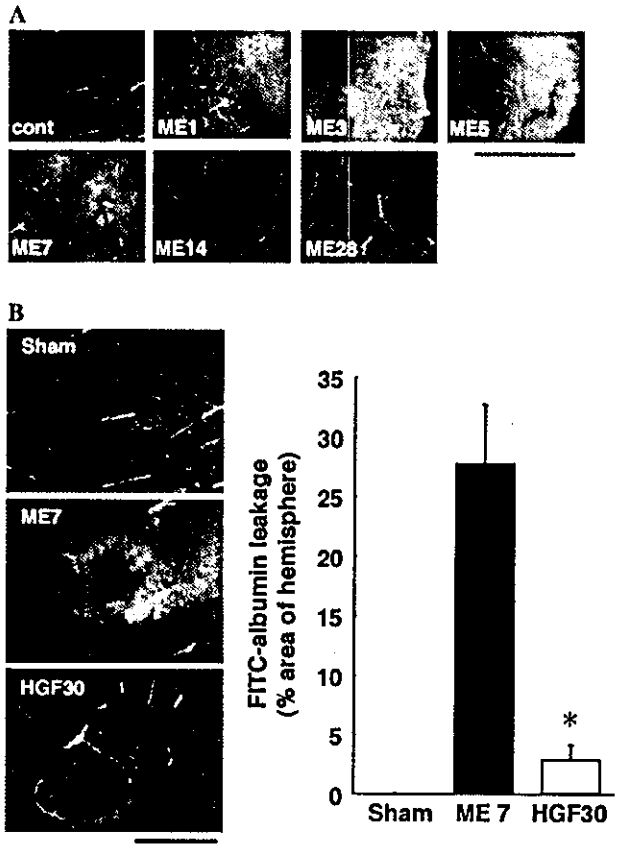

Fig. 3. E ect of hrHGF on the FITC–albumin leakage after the embolism. (A) Time course of changes in FITC–albumin leakage of the naive control (Cont) and hrHGF-untreated ME rat on days 1, 3, 5, 7, 14, and 28 after the operation. Bar, 50 μm. (B) E ect of hrHGF on the FITC–albumin leakage in the hrHGF-untreated (ME7) and 30 μg/7 days/animal hrHGF-treated ME (HGF30) rats on day 7 after the operation. Left panels are typical microphotographs of FITC–albumin leakage of the sham-operated (Sham), hrHGF-untreated ME (ME7), and hrHGF-treated ME (HGF30) rats. Bar, 50 μm. Each value for area of FITC–albumin leakage represents the mean percentage of total area of the ipsilateral hemisphere SEM ($n = 4$ each). The symbol * represents significant di erence from the hrHGF-untreated ME rats ($p < 0.05$).

FITC–albumin into the carotid arteries. Fig. 3A shows the time course of changes in FITC–albumin leakage in the ipsilateral cortex after the embolism. FITC–albumin leakage started on day 1 and lasted up to day 7 after the embolism. On the basis of this result, we next determined the e ect of treatment with hrHGF on FITC–albumin leakage on day 7 (Fig. 3B). In the ME rats, FITC–albumin leakage was seen in approximately 28% of the ipsilateral cerebral hemisphere, and treatment with hrHGF almost completely protected against it (Fig. 3B).

E ect of hrHGF on the number of TUNEL-positive vascular endothelial cells

To determine whether treatment with hrHGF protects the brain against injury to the endothelial cells after

the embolism, we next examined the e ect of hrHGF on the number of TUNEL-positive vascular endothelial cells in the ipsilateral cortex (Figs. 4A and B). The number of TUNEL-positive vascular endothelial cells was increased on day 3 after the embolism (Fig. 4A), and this increased number was significantly reduced by treatment with hrHGF (Figs. 4B and C).

E ect of hrHGF on the level of Bax, Bcl-xL, and Bcl-2

Finally, we determined the levels of apoptotic protein Bax and anti-apoptotic proteins Bcl-xL and Bcl-2 in the cerebral cortex on day 3 after the operation using immunoblotting analysis (Figs. 4D–F). The level of Bax protein in the cortex was not a ected by the embolism regardless of treatment or not with hrHGF (Fig. 4D). In contrast, the levels of Bcl-xL and Bcl-2 proteins were significantly decreased in the ME rats (Figs. 4E and F), and treatment with hrHGF attenuated the decrease in the level of Bcl-2 (Fig. 4F), but not that in the level of Bcl-xL protein (Fig. 4E).

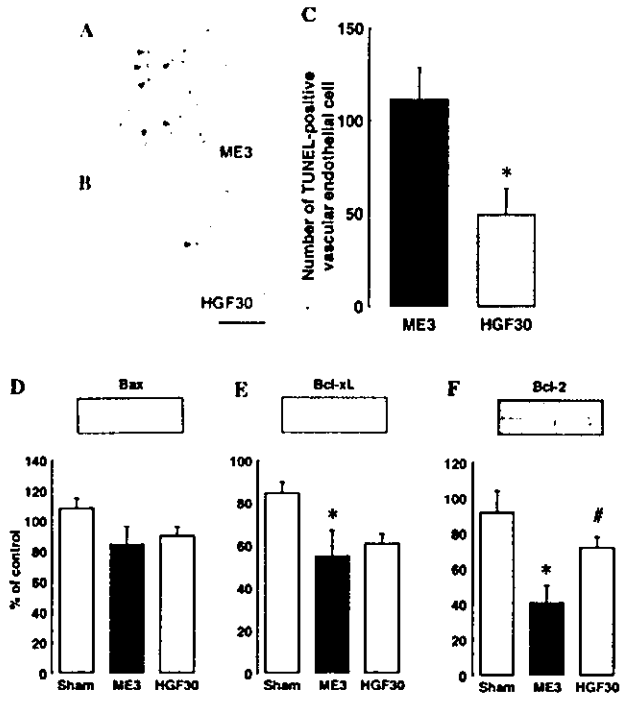

Fig. 4. E ect of hrHGF on the number of TUNEL-positive vascular endothelial cells after the embolism. (A,B) Photomicrographs of double staining for apoptotic cells (TUNEL; black, arrowheads) and von Willebrand factor (red) in the ipsilateral cortex of the hrHGF-untreated ME (ME3) and hrHGF-treated ME (HGF30) rats on day 3 after the operation. Bar, 50 μm. (C) The number of TUNEL-positive endothelial cells was counted in the ipsilateral cortex. Each value represents the mean SEM ($n = 4$ each). The symbol * represents significant di erence from the hrHGF-untreated ME rats ($p < 0.05$). E ect of hrHGF on the levels of Bax, Bcl-xL, and Bcl-2 in the cerebral cortex after the embolism. Representative immunoblots and their quantified data for Bax (D), Bcl-xL (E), and Bcl-2 (F) of the sham-operated (Sham), hrHGF-untreated ME (ME), and hrHGF-treated ME (HGF30) rats on day 3 after the operation are shown. Each value represents the mean percentage of the naive control SEM ($n = 3$ each). The symbol * represents significant di erence from the sham-operated rats ($p < 0.05$); The symbol # represents significant di erence from the hrHGF-untreated ME rats ($p < 0.05$).

Discussion

Microsphere embolism-induced sustained cerebral ischemia caused a spatial learning dysfunction. Cerebral ischemia induced by four-vessel occlusion [23,24] or middle cerebral artery occlusion [25,26] in rodents has been shown to induce learning and memory dysfunction in the water maze test. Although the degree of severity in learning and memory dysfunction that we observed would not compare simply with that of other models, the failure of spatial memory function of the ME animals seems to be more long-lasting than that in the other models described above. This di erence could be possibly due to the severity of the microsphere embolism model, for it involves irreversible, widespread, and small embolic multi-infarcts, especially in the cerebral cortex and hippocampus [14]. We demonstrated that treatment with hrHGF dose-dependently improved acquisition of spatial learning and memory impaired by sustained cerebral ischemia. To further examine the e ect of HGF on the spatial navigation ability, we conducted the retention test on days 21 and 28 after the operation. It is noteworthy that hrHGF-treated ME animals revealed significant shortening of the escape latency in the retention test. These findings are the first evidence to demonstrate that HGF has the ability to exert a persistent e ect on the learning and memory function of animals with sustained cerebral ischemia.

The question arises as to the nature of the mechanism underlying the HGF-mediated improvement of learning and memory function after sustained cerebral ischemia. In the ischemic brain, the most important pathological event that contributes to the impairment of brain function is the shortage of glucose and oxygen supply for the brain tissue. Therefore, e cient vascular supply of blood is capable of preventing the progression of ischemic pathogenesis, including cerebral infarction and tissue degeneration, and may correlate with functional recovery after cerebral ischemia. Treatment with hrHGF significantly prevented the tissue degeneration. Therefore, HGF may prevent injury to plasma-perfused vessels, consequently maintaining glucose and oxygen supply to brain tissue, possibly to the penumbra. In addition to the e ect of HGF on the cerebral vessels, HGF might directly attenuate ischemia-induced neuronal cell death. In this sense, it has previously been shown that HGF reduced infarct volume by preventing apoptotic neuronal cell death of transiently middle cerebral artery-occluded rats [13].

To further elucidate the mechanisms for the protective e ects of HGF on leaning and memory function, we focused on the events at the early period after the embolism. After a stroke, disruption of the BBB appears to occur acutely [27,28]. The majority of brain injuries after a stroke are associated with disruption of the BBB, leading to secondary damage to neurons [29,30]. Indeed, disturbance of BBB permeability exacerbates cell damage after focal cerebral ischemia [28,31]. We demonstrated that FITC–albumin leakage started on day 1 and lasted up to day 7 after the embolism. This result was comparable to the finding that a significant increase in the BBB permeability occurred 48–72 h after middle cerebral artery occlusion [27,28]. Our findings led us to examine the e ects of hrHGF on the BBB leakage after the microsphere embolism. As a result, treatment with hrHGF almost completely protected against FITC–albumin leakage. As the structure of the BBB is a barrier comprising tight junctions localized in blood capillaries [32,33], it is possible that HGF attenuated ischemia-induced injury to the endothelial cell thereby resulting in prevention of BBB leakage.

To achieve further insight into the e ects of HGF on cerebral vessels after the embolism, we next performed immunohistochemical analysis of the cerebral endothelial cells. Our data demonstrated that the microsphere embolism-induced increase in the number of TUNEL-positive endothelial cells was attenuated by treatment with hrHGF. The result suggests that HGF acts on the endothelial cells and prevents apoptotic cell death, which leads to preservation of BBB integrity after microsphere embolism. With respect to this suggestion, we further demonstrated that treatment with hrHGF lessened the drop in the level of anti-apoptotic protein Bcl-2 without changing the amount of the apoptotic protein Bax. Thus, HGF may prevent injury to endothelial cells by anti-apoptotic action, although we cannot fully exclude the possibility that HGF might change the localization of Bax protein in the cells as seen in high D-glucose- and hypoxia/reoxygenation-induced endothelial cell apoptosis [34,35]. Since HGF also stimulates the migration of vascular smooth muscle cells, there remains the possibility that the protective e ect of HGF on the BBB contributes to HGF-induced simultaneous stimulation of the migration of both endothelial and vascular smooth muscle cells.

In conclusion, we demonstrated for the first time that HGF has the ability to prevent learning and memory dysfunction after sustained cerebral ischemia. The effects of HGF on perfused vessels and BBB appear to be mediated by prevention of endothelial cell injury, which possibly elicits a persistent supply of blood flow to the penumbra. As HGF has a potent cerebroprotective effect, it should be evaluated as a prospective agent for the therapy against ischemic brain injuries, including cerebral infarction and vascular dementia.

Acknowledgments

This work was supported by a Grant-in-Aid from Ministry of Education, Science, Sports and Culture of Japan.

References

[1] T. Nakamura, K. Nawa, A. Ichihara, Partial purification and characterization of hepatocyte growth factor from serum of hepatectomized rats, Biochem. Biophys. Res. Commun. 122 (1984) 1450–1459.
[2] T. Nakamura, T. Nishizawa, M. Hagiya, T. Seki, M. Shimonishi, A. Sugimura, K. Tashiro, S. Shimizu, Molecular cloning and expression of human hepatocyte growth factor, Nature 342 (1989) 440–443.
[3] R. Zarnegar, G.K. Michalopoulos, The many faces of hepatocyte growth factor: from hepatopoiesis to hematopoiesis, J. Cell Biol. 129 (1995) 1177–1180.
[4] K. Matsumoto, T. Nakamura, Emerging multipotent aspects of hepatocyte growth factor, J. Biochem. 119 (1996) 591–600.
[5] D.F. Balkovetz, J.H. Lipschutz, Hepatocyte growth factor and the kidney: it is not just for the liver, Int. Rev. Cytol. 186 (1999) 225–260.
[6] K. Matsumoto, T. Nakamura, Hepatocyte growth factor: renotropic role and potential therapeutics for renal diseases, Kidney Int. 59 (2001) 2023–2038.
[7] T. Nakamura, S. Mizuno, K. Matsumoto, Y. Sawa, H. Matsuda, T. Nakamura, Myocardial protection from ischemia/reperfusion injury by endogenous and exogenous HGF, J. Clin. Invest. 106 (2000) 1511–1519.
[8] E. Van Belle, B. Witzenbichler, D. Chen, M. Silver, L. Chang, R. Schwall, J.M. Isner, Potentiated angiogenic e ect of scatter factor/hepatocyte growth factor via induction of vascular endothelial growth factor: the case for paracrine amplification of angiogenesis, Circulation 97 (1998) 381–390.
[9] R. Morishita, S. Nakamura, S. Hayashi, Y. Taniyama, A. Moriguchi, T. Nagano, M. Taiji, H. Noguchi, S. Takeshita, K. Matsumoto, T. Nakamura, J. Higaki, T. Ogihara, Therapeutic angiogenesis induced by human recombinant hepatocyte growth factor in rabbit hind limb ischemia model as cytokine supplement therapy, Hypertension 33 (1999) 1379–1384.
[10] S. Honda, M. Kagoshima, A. Wanaka, M. Tohyama, K. Matsumoto, T. Nakamura, Localization and functional coupling of HGF and c-Met/HGF receptor in rat brain: implication as neurotrophic factor, Brain Res. Mol. Brain Res. 32 (1995) 197–210.
[11] C.L. Achim, S. Katyal, C.A. Wiley, M. Shiratori, G. Wang, E. Oshika, B.E. Petersen, J.M. Li, G.K. Michalopoulos, Expression of HGF and cMet in the developing and adult brain, Brain Res. Dev. Brain Res. 102 (1997) 299–303.
[12] T. Miyazawa, K. Matsumoto, H. Ohmichi, H. Katoh, T. Yamashima, T. Nakamura, Protection of hippocampal neurons from ischemia-induced delayed neuronal death by hepatocyte growth factor: a novel neurotrophic factor, J. Cereb. Blood Flow Metab. 18 (1998) 345–348.
[13] N. Tsuzuki, T. Miyazawa, K. Matsumoto, T. Nakamura, K. Shima, Hepatocyte growth factor reduces the infarct volume after transient focal cerebral ischemia in rats, Neurol. Res. 23 (2001) 417–424.
[14] K. Miyake, S. Takeo, H. Kajihara, Sustained decrease in brain regional blood flow after microsphere embolism in rats, Stroke 24 (1993) 415–420.
[15] P.D. Lyden, J.A. Zivin, D.R. Chabolla, M.A. Jacobs, F.H. Gage, Quantitative e ects of cerebral infarction on spatial learning in rats, Exp. Neurol. 116 (1992) 122–132.

[16] H. Naritomi, Experimental basis of multi-infarct dementia: memory impairments in rodent models of ischemia, Alzheimer Dis. Assoc. Disord. 5 (1991) 103–111.
[17] N. Takagi, K. Miyake, T. Taguchi, H. Tamada, K. Takagi, N. Sugita, S. Takeo, Failure in learning task and loss of cortical cholingergic fibers in microsphere-embolized rats, Exp. Brain Res. 114 (1997) 279–287.
[18] A. Nagakura, K. Miyake-Takagi, N. Takagi, M. Fukui, S. Takeo, Impairment of adenylyl cyclase and of spatial memory function after microsphere embolism in rats, J. Neurosci. Res. 68 (2002) 363–372.
[19] T. Seki, I. Ihara, A. Sugimura, M. Shimonishi, T. Nishizawa, O. Asami, M. Hagiya, T. Nakamura, S. Shimizu, Isolation and expression of cDNA for di erent forms of hepatocyte growth factor from human leukocyte, Biochem. Biophys. Res. Commun. 172 (1990) 321–327.
[20] T.W. Furlow, N.H. Bass, Arachidonate-induced cerebrovascular occlusion in the rat. The role of platelets and aspirin in stroke, Neurology 26 (1976) 297–304.
[21] C.P. McGraw, Experimental cerebral infarction e ects of pentobarbital in Mongolian gerbils, Arch. Neurol. 34 (1977) 334–336.
[22] M. Cavaglia, S.M. Dombrowski, J. Drazba, A. Vasanji, P.M. Bokesch, D. Janigro, Regional variation in brain capillary density and vascular response to ischemia, Brain Res. 910 (2001) 81–93.
[23] H. Hodges, Maze procedures: the radial-arm and water maze compared, Cogn. Brain Res. 3 (1996) 167–181.
[24] T. Imanishi, A. Sawa, Y. Ichimaru, M. Miyashiro, S. Kato, T. Yamamoto, S. Ueki, Ameliorating e ects of rolipram on experimentally induced impairments of learning and memory in rodents, Eur. J. Pharmacol. 321 (1997) 273–278.
[25] F. Yonemori, T. Yamaguchi, H. Yamada, A. Tamura, Spatial cognitive performance after chronic focal cerebral ischemia in rats, J. Cereb. Blood Flow Metab. 19 (1999) 483–494.
[26] M. Modo, R.P. Stroemer, E. Tang, T. Veizovic, P. Sowniski, H. Hodges, Neurological sequelae and long-term behavioural assessment of rats with transient middle cerebral artery occlusion, J. Neurosci. Methods 104 (2000) 99–109.
[27] O. Gotoh, T. Asano, T. Koide, K. Takakura, Ischemic brain edema following occlusion of the middle cerebral artery in the rat. I: The time courses of the brain water, sodium and potassium contents and blood–brain barrier permeability to ^{125}I-albumin, Stroke 16 (1985) 101–109.
[28] L. Belayev, R. Busto, W. Zhao, M.D. Ginsberg, Quantitative evaluation of blood–brain barrier permeability following middle cerebral artery occlusion in rats, Brain Res. 739 (1996) 88–96.
[29] M.A. Petty, J.G. Wettstein, Elements of cerebral microvascular ischaemia, Brain Res. Rev. 36 (2001) 23–34.
[30] S. Nag, The blood–brain barrier and cerebral angiogenesis: lessons from the cold-injury model, Trends Mol. Med. 8 (2002) 38–44.
[31] J.V. Bounds, D.O. Wiebers, J.P. Whisnant, H. Okazaki, Mechanisms and timing of deaths from cerebral infarction, Stroke 12 (1981) 474–477.
[32] W. Risau, Di erentiation of endothelium, FASEB J. 9 (1995) 926–933.
[33] W. Risau, H. Wolburg, Development of the blood–brain barrier, Trends Neurosci. 13 (1990) 174–178.
[34] H. Nakagami, R. Morishita, K. Yamamoto, Y. Taniyama, M. Aoki, K. Yamasaki, K. Matsumoto, T. Nakamura, Y. Kaneda, T. Ogihara, Hepatocyte growth factor prevents endothelial cell death through inhibition of bax translocation from cytosol to mitochondrial membrane, Diabetes 51 (2002) 2604–2611.
[35] X. Wang, Y. Zhou, H.P. Kim, R. Song, R. Zarnegar, S.W. Ryter, A.M. Choi, Hepatocyte growth factor protects against hypoxia/reoxygenation-induced apoptosis in endothelial cells, J. Biol. Chem. 279 (2004) 5237–5243.